Balancing Efficiency and Expressiveness: Subgraph GNNs with Walk-Based Centrality

Joshua Southern [*1] **Yam Eitan** [2] **Guy Bar-Shalom** [2] **Michael M. Bronstein** [3 4] **Haggai Maron** [2 5]
Fabrizio Frasca [*2]

Abstract

Subgraph GNNs have emerged as promising architectures that overcome the expressiveness limitations of Graph Neural Networks (GNNs) by processing bags of subgraphs. Despite their compelling empirical performance, these methods are afflicted by a high computational complexity: they process bags whose size grows linearly in the number of nodes, hindering their applicability to larger graphs. In this work, we propose an effective and easy-to-implement approach to dramatically alleviate the computational cost of Subgraph GNNs and unleash broader applications thereof. Our method, dubbed HyMN, leverages walk-based centrality measures to sample a small number of relevant subgraphs and drastically reduce the bag size. By drawing a connection to perturbation analysis, we highlight the strength of the proposed centrality-based subgraph sampling, and further prove that these walk-based centralities can be additionally used as Structural Encodings for improved discriminative power. A comprehensive set of experimental results demonstrates that HyMN provides an effective synthesis of expressiveness, efficiency, and downstream performance, unlocking the application of Subgraph GNNs to dramatically larger graphs. Not only does our method outperform more sophisticated subgraph sampling approaches, it is also competitive, and sometimes better, than other state-of-the-art approaches for a fraction of their runtime.

[*]Equal technical contribution [1]Imperial College London [2]Technion – Israel Institute of Technology [3]University of Oxford [4]AITHYRA [5]NVIDIA Research. Correspondence to: Joshua Southern <jks17@ic.ac.uk>, Fabrizio Frasca <fabriziof@campus.technion.ac.il>.

Proceedings of the 42nd International Conference on Machine Learning, Vancouver, Canada. PMLR 267, 2025. Copyright 2025 by the author(s).

1. Introduction

Graph Neural Networks (GNNs) (Scarselli et al., 2009; Gori et al., 2005; Micheli, 2009) have achieved great success in learning tasks with graph-structured data. Typically, GNNs are based on the message passing paradigm (Gilmer et al., 2017), in which node features are aggregated over their local neighborhood recursively, resulting in architectures known as Message Passing Neural Networks (MPNNs). MPNNs have been shown to suffer from limited expressive power: they are bounded by 1-WL (Xu et al., 2018; Geerts & Reutter, 2023; Weisfeiler & Leman, 1968; Morris et al., 2019; 2023) cannot count certain substructures (Chen et al., 2020; Bouritsas et al., 2022; Tahmasebi et al., 2020) or solve graph bi-connectivity tasks (Zhang et al., 2023b).

Recently, Subgraph GNNs (Bevilacqua et al., 2021; Frasca et al., 2022; Zhang & Li, 2021; Cotta et al., 2021) have been proposed to overcome some of the expressivity limitations of MPNNs. This approach preserves equivariance while relying less on feature engineering. First, a Subgraph GNN transforms a graph into a "bag of subgraphs" based on a specific selection policy. These subgraphs are then processed by an equivariant architecture and aggregated to make graph- or node-level predictions. One common approach to generate subgraphs, known as node-marking, is to mark a single node in the graph (Papp & Wattenhofer, 2022). In this case, each subgraph is then "tied" to a specific node in the original graph, and a shared MPNN generates a representation for each subgraph.

In general, Subgraph GNNs show good empirical performance but come with a high computational cost. For a graph of N nodes and a maximum degree d_{max}, then Subgraph GNNs with node-marking based policies have a computational complexity $O(N^2 \cdot d_{\mathsf{max}})$. To reduce computational complexity, it was suggested sampling subgraphs randomly (Bevilacqua et al., 2021; Zhao et al., 2022) or, more recently, learning sampling policies (Qian et al., 2022; Bevilacqua et al., 2024; Kong et al., 2024). However, while random approaches have been shown to be suboptimal (Bevilacqua et al., 2024; Bar-Shalom et al., 2024b), learnable policies are difficult to train in practice and become impractical when sampling a larger number of sub-

graphs, due to the use of discrete sampling and RL-based objectives.

Summarizing, while Subgraph GNNs have demonstrated promising results on small molecular graphs, their computational requirements make them impractical for graphs larger than a few tens of nodes. This severe limitation needs to be addressed in an effective way to broaden the application of these models.

Our approach. In this work, we present an approach that drastically reduces the complexity of Subgraph GNNs while maintaining their competitive performance. We achieve this by identifying easy-to-compute structural features that unlock a simple yet effective subgraph selection strategy, while providing complementary information enhancing the model's expressiveness.

We first identify a family of node centrality measures (Estrada & Rodriguez-Velazquez, 2005; Benzi & Klymko, 2013; 2014) as easy-to-compute scores that: (i) recapitulate well the extent to which a subgraph alters the graph representation; (ii) correlate with relevant substructure counts. In light of this, we propose to leverage these measures to efficiently and effectively reduce the size of bags of subgraphs without requiring additional learnable components. Specifically, we prioritize selecting marked subgraphs associated with the top-ranking nodes according to these centrality measures and, in particular, to the Subgraph Centrality by Estrada & Rodriguez-Velazquez (2005). Then, we propose to additionally interpret centrality scores as Structural Encodings (SEs) (Bouritsas et al., 2022; Dwivedi et al., 2021; Fesser & Weber, 2024), and to utilize them to augment the node features of the selected subgraphs. This combination of approaches is justified from an expressiveness perspective, as we show neither of the two subsume the other. We demonstrate node marking of (selected) subgraphs separates graphs that are not separable by Centrality-based SE (CSE) feature augmentations *and*, vice-versa, that CSEs allow to separate pairs indistinguishable to our subsampled Subgraph GNNs.

The resulting method, dubbed HyMN (*Hybrid Marking Network*), is an approach whereby Subgraph GNNs and Structural Encodings work in tandem to effectively overcome the expressiveness limitations of MPNNs and unlock the application of Subgraph GNNs to larger graphs previously out of reach. Our approach is provably expressive, does not require feature engineering or learnable sampling components, and, importantly, maintains a low computational cost. The practical value of our approach is confirmed by the strong results achieved over a series of experimental analyses conducted over synthetic and real-world benchmarks. We show HyMN outperforms other subgraph selection strategies, and performs on par or better than full-bag Subgraph GNNs by only sampling one or two subgraphs. Additionally, HyMN is competitive to (and sometimes better than) Graph Transformers and other state-of-the-art GNNs, while, as we show through extensive wall-clock timing analyses, features a dramatically reduced computational runtime.

Our **contributions** are summarized as follows:

1. We show that walk-based node centrality measures and, in particular, the Subgraph Centrality of Estrada & Rodriguez-Velazquez (2005), represent a simple and effective indicator of subgraph importance for subsampling bags in Subgraph GNNs.
2. We demonstrate that centrality-based structural features can be employed as Structural Encodings to enhance the discriminative power of Subgraph GNNs with subsampled bags of subgraphs.
3. We provide strong experimental evidence showcasing the effectiveness of our sampling strategy and the efficacy of additionally incorporating centrality-based SEs.
4. We show how our approach enables subgraph-methods to scale to substantially larger graphs than previously possible, even tens or hundreds of times larger.

Overall, our results validate our method as a simple, expressive and efficient approach that competes with state-of-the-art GNNs for a fraction of their empirirical run-times.

2. Related Work

Expressive power of MPNNs. The expressive power of MPNNs has become a central research topic since they were shown to be bounded by the 1-WL isomorphism test (Morris et al., 2019; Xu et al., 2018; Morris et al., 2023). This has led to approaches which aim to obtain different representations for non-isomorphic but 1-WL equivalent graphs. These include using random features (Sato et al., 2021; Abboud et al., 2021), higher-order message passing schemes (Bodnar et al., 2021b;a; Morris et al., 2019; 2020b) and equivariant models (Maron et al., 2018; Vignac et al., 2020). One of the most common approaches is to inject positional and structural encodings into the input layer (Bouritsas et al., 2022; Fesser & Weber, 2024; Dwivedi et al., 2021; Kreuzer et al., 2021) using Laplacian PEs (Dwivedi & Bresson, 2021; Kreuzer et al., 2021; Wang et al., 2022; Lim et al., 2023; 2024), distance information (Ying et al., 2021; Li et al., 2020), or random-walk encodings (RWSE) (Dwivedi et al., 2021).

Subgraph GNNs. A recent line of work has proposed representing a graph as a collection of subgraphs obtained by a specific selection policy (Zhang & Li, 2021; Cotta et al., 2021; Papp & Wattenhofer, 2022; Bevilacqua et al., 2021; Zhao et al., 2022; Papp et al., 2021; Frasca et al., 2022; Qian et al., 2022; Huang et al., 2023; Zhang et al., 2023a). These

approaches, jointly referred to as Subgraph GNNs, allow to overcome the expressivity limitations of MPNNs without introducing predefined encodings. A powerful, common selection policy termed *node marking* involves generating a subgraph per node by marking that node in the original graph, with no connectivity alterations. Although it can increase expressive power beyond 1-WL (Frasca et al., 2022; You et al., 2021), this approach has a high complexity as it needs to consider and process N different subgraphs, N being the number of nodes in the original graph.

Scaling Subgraph GNNs. Several recent papers have focused on scaling these methods to larger graphs. Beyond random sampling (Bevilacqua et al., 2021; Zhao et al., 2022), Qian et al. (2022) first proposed gradient-based techniques to *learn* how to subsample the bag of subgraphs. Bevilacqua et al. (2024) introduced *Policy-Learn* (PL), which iteratively predicts a distribution over nodes in the graph and samples subgraphs from the full-bag accordingly. A similar approach, called MAG-GNN has also proposed to sample subgraphs using Reinforcement Learning (RL) (Kong et al., 2024). Both of these approaches involve *discrete sampling* which can complicate the training process, often requiring $1,000-4,000$ training epochs. Another recent approach leverages the connection between Subgraph GNNs and graph products (Bar-Shalom et al., 2024a) to run message passing on the product of the original graph and a coarsened version thereof (Bar-Shalom et al., 2024b). The control over the computational complexity generally comes from the existence of cluster-like structures in the graph which, however, may not be aligned with the preset number of subgraphs. Additionally, the locality bias afforded by the coarsening may not generally be effective across tasks. In such cases, coarsening approaches that are not learnable and based, e.g., on spectral clustering could lead to suboptimal results. For an extended background on Subgraph GNNs, the node marking policy and efforts around scaling this family of architectures, we refer readers to Appendix B.

Node Centrality. One common way to characterize nodes in a graph is by using the concept of *node centrality*. A node centrality measure defines a real-valued function on the nodes, $c : V \to \mathbb{R}$, which can be used to rank nodes within a network by their "importance". Different concepts of importance have led to a myriad of measures in the Network Science community. They range from the simple Degree Centrality (central nodes have the highest degrees) to path-based methods (Freeman, 1977) like the Betweenness Centrality (central nodes fall on the shortest paths between many node-pairs). An important family of centrality measures quantifies the importance of nodes based on *walk counts*. As noted in (Benzi & Klymko, 2014), most of these measures take the form of a power series, where numbers of walks for any lengths are aggregated with an appropriate discounting scheme. Prominent examples include the Katz Index (Katz, 1953) (KI) and the Subgraph Centrality (Estrada & Rodriguez-Velazquez, 2005) (SC):

$$c_i^{\text{KI}} = \sum_{k=0}^{\infty} \alpha^k \sum_j (A^k)_{ij} \qquad c_i^{\text{SC}} = \sum_{k=0}^{\infty} \frac{\beta^k}{k!} (A^k)_{ii} \quad (1)$$

and variants of the above, for appropriate choices of $0 < \alpha < \frac{1}{\lambda_1}, \beta > 0$[1] (Benzi & Klymko, 2013; 2014). By scoring nodes based on the cumulative number of walks that start from them, these centrality measures extend the Degree Centrality beyond purely local interactions, in a way that depends on the discounting scheme (α^k and $\frac{\beta^k}{k!}$ for KI and SC, respectively).

3. Subsampling Subgraph Neural Networks

3.1. Problem Setting

We focus on Subgraph GNNs with a node-marking selection policy (Papp & Wattenhofer, 2022; You et al., 2021). Given an N-node graph $G = (A, X)$, a node-marking Subgraph GNN processes a bag of subgraphs obtained from G, viz. $B_G = \{\!\{S_1, S_2, \ldots, S_N\}\!\}$. Here, $S_i = (A, X_i)$ and $X_i = X \oplus x_{v_i}$, where $\oplus$ denotes channel-wise concatenation and x_{v_i} is a one-hot indicator vector for node v_i.

Goal. In order to reduce the computational complexity of a Subgraph GNN, we aim to reduce the size of the bag by *efficiently and effectively* sampling $k < N$ subgraphs. The sampling procedure must be *efficient* in that it should avoid computationally complex operations or the use of learnable components requiring more involved training protocols (Qian et al., 2022; Bevilacqua et al., 2024; Kong et al., 2024). Ideally, it should consist of a simple and lightweight preprocessing step prior to running a chosen Subgraph GNN. The sampling procedure must additionally be *effective*, which means it should closely approach the performance of a full-bag Subgraph GNN with as few subgraphs as possible. Put differently, it should prioritize marking those nodes that most quickly lead to performance improvements. As an example, to ground the discussion: randomly selecting subgraphs (Bevilacqua et al., 2021; Papp et al., 2021) is an efficient but not effective strategy; learning which subgraph to mark via RL (Kong et al., 2024) is a more effective approach, but it may not be efficient enough.

We start by presenting considerations on effectiveness which will naturally lead us to focus on walk-based centrality measures for our purposes. Upon them, we show we can build an effective strategy that is also efficiently executed as a simple preprocessing step.

[1] λ_1 refers to the first eigenvalue of A, β is typically set to 1.

3.2. Effective Node Marking

What makes a node a good marking candidate? We propose approaching this question by considering *node marking as a graph perturbation*. Marking a node changes the initial node features: this alteration in the input will ultimately be reflected in the output graph representation, and understanding how node marking impacts the output graph representation is instrumental in designing effective sampling strategies. Beyond binary graph separation, we claim that an effective marking should be able to (i) alter graph representations sufficiently; (ii) induce perturbations that correlate with graph targets. Ideally, when marking nodes jointly optimizes (i) and (ii), a Subgraph GNN with a small bag can then improve on a standard MPNN by sufficiently separating more graphs and in a way that assists the training objective.

Node Marking, perturbations, and centrality measures. To understand how marking a node alters graphs representations, we analyze the simplest case: marking a single node. In particular, we ask how much the representation of a generic graph G can be changed by a single-node marking. As the MPNN, we consider an L-layer GIN (Xu et al., 2018; Chuang & Jegelka, 2022):

$$h_v^{(l)} = \phi^{(l)}\big(h_v^{(l-1)} + \epsilon \sum_{u \in N(v)} h_u^{(l-1)}\big),\ y_G = \phi^{(L+1)}\big(\sum_{v \in G} h_v^{(L)}\big) \tag{2}$$

where $\phi^{(l)}$'s are update functions and $\phi^{(L+1)}$ is a prediction layer (all are parameterized as MLPs). By applying results from GNN stability studies in (Chuang & Jegelka, 2022) we put forward the following observation (see details in Appendix E):

Observation 1. The distance between the MPNN representations of a graph G and a graph S_v generated by marking node v in G, can be upper-bounded as:

$$|y_G - y_{S_v}| \leq \prod_{l=1}^{L+1} K_\phi^{(l)} \cdot \underbrace{\sum_{l=1}^{L+1} \lambda_l \cdot \sum_j (A^{l-1})_{v,j}}_{(\mathcal{A})} \tag{3}$$

where K_ϕ^l is the Lipschitz constant of MLP $\phi^{(l)}, l = 1 \ldots L+1$, A is the adjacency matrix of graph G and $\lambda_l \in \mathbb{R}^+$ is an ϵ-dependent layer-wise weighting scheme.

Effectively, the cumulative number $(\mathcal{A})$ of walks starting from node v contributes to upper-bound the perturbation that marking v induces on the original graph representation. Hence, marking nodes involved in a lower number of walks will have a more limited influence on altering a message passing-based graph representation.

We note that the above observation uncovers an intriguing alignment with walk-based centrality measures: the "most important" nodes associate with the largest (discounted) cumulative numbers of walks (compare Equations 1 with term $(\mathcal{A})$ in Equation (3)). This leads us to direct our focus to walk-based centrality measures as promising candidates for selecting which node to mark. Considering we would like to sufficiently alter the graph representation beyond the one from a standard MPNN, Observation 1 indicates that, among all possible nodes, those associated with small cumulative numbers of walks will be poor marking candidates. We propose to summarise this form of information via walk-based centrality measures. Our strategy will be to *rank nodes based on their centrality values, and mark the top-scoring ones*. Next, we empirically verify the validity of this approach, and defer readers to Appendix E for extensions and more considerations on the above analysis.

High-centrality marking induces the largest perturbations. As a first experiment, we examine the extent to which node centralities recapitulate the amount of perturbation induced by marking their corresponding nodes. We consider the same setting discussed above: marking one node to transition from G to S_v, where S_v is obtained from G by marking node v. For a centrality measure c, we consider three cases: v attains the minimum of c (i), the maximum of c (ii), is randomly picked (iii). In each of these cases, we measured the distance $\|f(S_v) - f(G)\|$ on 100 graphs from two different real-world datasets from the popular TU suite: MUTAG and NCI1 (Morris et al., 2020a). Here, f is an untrained 3-layer GIN (Xu et al., 2018). Figure 1 and Figure 7a show results for the walk-based Subgraph Centrality (Estrada & Rodriguez-Velazquez, 2005), where horizontal lines indicate the average representation distance, and (i), (ii), (iii) are color-coded, resp., in green, blue, red.

From the plots, it is clearly visible how marking nodes with the lowest centrality leads to the smallest change in graph representation. This result gives direct empirical validation to the upper-bound analysis and the consequential observation discussed above. In accordance with our claim, subgraphs associated with low centrality nodes can be interpreted as poor marking candidates. Second, we note that marking nodes with the highest centrality induces the highest average perturbations, above random marking. This result is particularly relevant as it complements the above theoretical analysis: the walk-based upper-bound (Equation (3)) only suggests, but does not necessarily entail, that high-centrality marking associates with the largest perturbations. Figure 1 and Figure 7a show that this occurs in practice on these datasets, further motivating our proposed sampling strategy. Results for other centrality measures are found in Appendix F; they indicate that high-centrality marking leads, in all cases, to larger perturbations than random marking, with the highest values attained by walk-based centrality measures (see Section 2).

High-centrality marking aligns with substructure counting. We have shown how marking nodes with higher cen-

trality can lead to larger graph perturbations. However, this may not be sufficient. As an example, consider, two (non-isomorphic but) 1-WL-equivalent graphs. Node marking can alter their message-passing-based representations, but not necessarily in a way to induce separation: ideally, if the two graphs are associated with different targets we aim to induce *dissimilar perturbations* so to assist the training goal. In effect, we want our sampling strategy to alter the graph representations in a way that is consistent with the target space. Motivated by the observation that the presence and number of structural "motifs" are often related to graph-level tasks (Kanatsoulis & Ribeiro, 2024), we empirically study how marking-induced perturbations correlate with counting small substructures, as a general, yet relevant, predictor for graph-level targets.

We randomly generate 100 Erdös-Renyi (ER) graphs, each with $N = 20$ nodes and wiring probability $p = 0.3$. Similarly as above, we experiment with various centrality measures, by marking a single node v which attains either the maximum or minimum centrality value, or is randomly picked. Again, we record the perturbation $\|f(S_v) - f(G)\|$ given by the same architecture described above. On the same graphs, we count the number of various substructures, and evaluate the correlation between this value and the recorded perturbations. Results are reported in Table 1, expressed in terms of the Pearson correlation coefficient. Higher coefficients indicate substructure counts are better recapitulated by the perturbations induced by a certain marking strategy.

The top section of the table compares the correlations obtained by marking randomly or based on the Subgraph Centrality. The perturbations induced by high-centrality marking correlate significantly more with the considered substructures than those induced by low-centrality-based or random marking. The bottom section of the table presents results for other centralities not based on walks. We note how they all deliver better correlations w.r.t. random marking, but not as high as those attained by the SC.

Discussion. Overall our experiments indicate the following. First, *high-centrality sampling* shows to be a better approach than random sampling, especially when walk-based centrality measures are employed: on average, it selects marking candidates inducing the largest amount of perturbations over the original graph representations, and in a way that correlates with counts of relevant graph substructures. Second, the walk-based SC stands out as a particularly promising candidate: it is efficient to precalculate this measure and sample subgraphs based on that, while, on average, it performed as the best one in the experiments discussed above. In the following, we will focus on this measure in particular. Our strategy will consist of marking only the top-ranking k nodes according to SC, for a small, fixed k. As we will show, this simple approach already delivers strong empirical performance. More sophisticated sampling schemes could be designed based on extensions of the above analyses. These could consider more complex Subgraph GNN architectures (Frasca et al., 2022; Zhang et al., 2023a) or study the effect of multiple node markings, for which a deeper inquiry could take into account pair-wise scores beyond node-wise centrality measures[2]. We defer these efforts to future work.

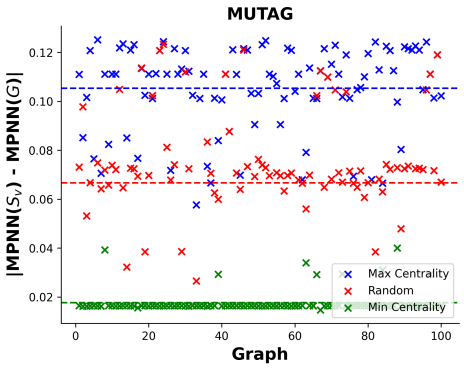

Figure 1: Plot showing the amount the graph representation using GIN is altered in the MUTAG dataset by adding an additional node-marked subgraph with (i) the highest centrality, (ii) the lowest centrality and (iii) a random marking.

Table 1: Pearson correlation between substructure counts and perturbation caused by different node-marking policies.

Method	Tri (↑)	4-Cyc (↑)	Tailed Tri (↑)	Star (↑)
Max Subgraph Centrality	**0.947**	**0.956**	**0.958**	**0.972**
Min Subgraph Centrality	0.644	0.643	0.634	0.698
Random	0.712	0.708	0.723	0.723
Max Degree Centrality	0.937	0.947	0.948	0.962
Max Closeness Centrality	0.935	0.937	0.946	0.957
Max Betweenness Centrality	0.803	0.816	0.821	0.845

4. Combining Subgraph GNNs with SEs

4.1. Our Approach

Subgraph Centrality as a SE. In Section 3, we introduced the use of walk-based centrality measures, particularly Subgraph Centrality, as an efficient and effective method for subgraph sampling. These centrality measures can be expressed as power series expansions of the adjacency matrix (Benzi & Klymko, 2014) (see Equation (1)). We notice that addenda terms in the series already provide precious discriminative structural information, which could be desirable to employ for feature augmentations (Rampášek et al., 2022; Bouritsas et al., 2022; Dwivedi et al., 2021). Precisely, in the case of our chosen Subgraph Centrality, for the default $\beta = 1$, the k-th term $\frac{(A^k)_{vv}}{k!}$ is (the discounted number of) k-length closed-walks originating from v. As notable

[2]For example, when selecting multiple nodes to mark, one could also account for the distance between them.

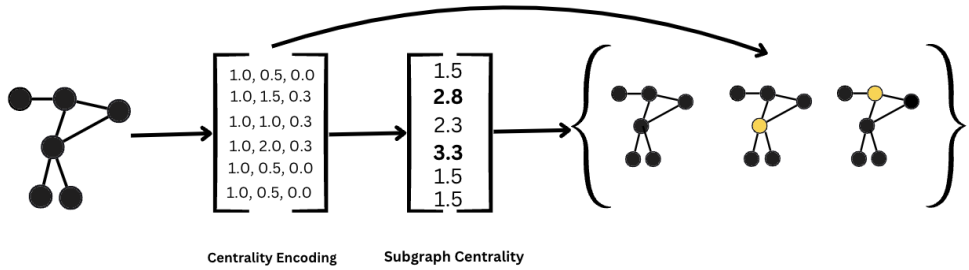

Figure 2: An overview of the pipeline for HyMN. We calculate the CSE for each node, sample T node-marked subgraphs with the highest Subgraph Centrality and concatenate the CSE with the initial node features.

examples, these values are proportional to the degree of v and the number of incident triangles for $k = 2, 3$. These considerations suggest retaining the intermediate values that contribute to the SC of each node, and employ them à la Structural Encodings beyond sampling purposes.

We naturally define the Centrality-based Structural Encodings (CSE) of order K for node v as[3]:

$$C_v^{\mathsf{CSE}} = \left[1, \frac{(A)^1_{vv}}{1!}, \frac{(A)^2_{vv}}{2!}, \frac{(A)^3_{vv}}{3!}, \ldots, \frac{(A)^K_{vv}}{K!}\right]. \quad (4)$$

As $K \to \infty$, the sum of these terms clearly coincides with the SC of the node for the default $\beta = 1$. We refer readers to Appendix F.5, for considerations on how CSEs compare with RWSEs.

Hybrid Marking Networks. Our overall method consists in *jointly* (1) augmenting node features with K-order CSEs; (2) subsampling the T node-marked subgraphs for the nodes attaining the highest centrality values; (3) processing the obtained bag of subgraphs with a Subgraph GNN of choice.

In view of (1) and (2), we dub our approach HyMN, as in *Hybrid Marking Network*. These steps are depicted in Figure 2 and described in Algorithm 1 (Appendix C). We note the following. First, for a large enough K, centrality values can be approximated by directly summing over the computed K-order CSEs. Second, node marking does not require any alteration of the original graph topology, making it unnecessary to store the subgraph connectivity. We thus opt not to materialize the bag of subgraphs: we only record marking information in the feature tensor and implement a custom message-function that processes it in an equivariant way. From an engineering standpoint, this allows for further memory-complexity enhancement w.r.t. generic Subgraph GNN approaches.

4.2. Expressivity of Subgraph GNNs with CSEs

HyMN effectively marries two distinct Graph Learning approaches: the use of node-marked subgraphs and of SEs. At this point, it is natural to ask whether this combination of techniques is justified from an expressiveness perspective. Put differently, we ask whether enhancing message passing with CSEs already subsumes our high-centrality marking strategy or, vice-versa, whether our marking approach could recover CSEs.

We answer these questions with graph separation arguments (Xu et al., 2018; Morris et al., 2019) and highlight how, in fact, the two approaches are not generally comparable. We demonstrate that subsampling Subgraph GNNs with high-centrality marking *does not* subsume CSE-enhanced MPNNs, while, at the same time, the discriminative power of the former approach *is not* fully captured by the latter. Since neither technique alone fully subsumes the other, our analysis emphasizes the advantages of combining them in HyMN for improved expressiveness. Proofs and additional details are reported in Appendix D.

MPNNs with centrality encoding do not subsume subsampled Subgraph GNNs. Below, we show that node-marked subgraphs can separate graphs indistinguishable by CSE-enhanced MPNNs, i.e., MPNNs running on graphs whose features are augmented with our centrality-based encodings.

Theorem 4.1. *There exists a pair of graphs G and G' such that for any CSE-enhanced MPNN model M_{CSE} we have $M_{CSE}(G) = M_{CSE}(G')$, but there exists a DS-Subgraph GNN model (without CSEs) $M_{sub.}$ which uses a top-1 Subgraph Centrality policy such that $M_{sub.}(G) \neq M_{sub.}(G')$.*

This result is proved, in particular, by considering two 1-WL equivalent graphs which have identical values for CSEs. This makes them indistinguishable by a CSE-enhanced MPNN, contrary to (sampled) DS-Subgraph GNNs (Bevilacqua et al., 2021), the simplest Subgraph GNN variants which process subgraphs independently. This underscores the advantage of incorporating a node-marking Subgraph GNN alongside structural encoding techniques.

Subsampled Subgraph GNNs do not subsume MPNNs with centrality encoding. Processing only a fixed number of subgraphs selected by our high-centrality strategy may limit discriminative power. In particular, the following

[3]We defined CSEs directly as the addenda in the power-series in Equation (1), but we note that the first two terms are not discriminative and could be dropped.

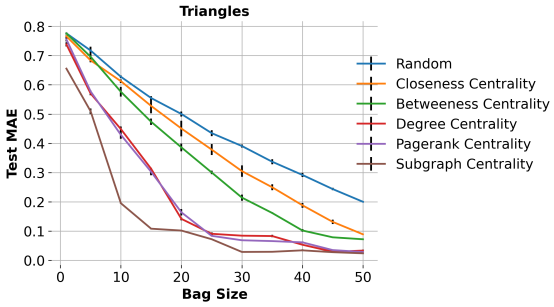

Figure 3: Comparing sampling approaches for counting triangles (performance metric is Mean Absolute Error, the lower the better). The average graph size is 59.33, corresponding to the average bag-size of a full-bag Subgraph GNN.

shows that this approach does not subsume CSE-enhanced MPNNs:

Theorem 4.2. *There exists a pair of graphs G and G' such that for* any *Subgraph GNN model $M_{sub.}$ which uses a top-1 Subgraph Centrality policy we have $M_{sub.}(G) = M_{sub.}(G')$, but there exists an MPNN + centrality encoding model M_{CSE} such that $M_{CSE}(G) \neq M_{CSE}(G')$.*

This result exposes a limitation of subsampled Subgraph GNNs in distinguishing between two non-isomorphic graphs with differing closed walks, features which are, instead, captured by CSEs. Notably, as discussed in Proposition D.5 (Appendix D), a *full-bag* approach is capable of capturing CSEs. This observation suggests that while CSEs do not universally enhance the expressiveness of any Subgraph GNN, they can be beneficial when subsampling a limited number of subgraphs.

Taken together, Theorems 4.1 and 4.2 indicate that leveraging SC both as a SE *and* as a means for subgraph sampling is advantageous in terms of discriminative power, justifying the integration of the two techniques in HyMN.

5. Experiments

Our experiments[4] aim to validate arguments in the previous sections and to empirically answer the following questions:

- (**Q1**) *Can SC be used to effectively subsample subgraphs for Subgraph GNNs?*
- (**Q2**) *Can HyMN efficiently scale to graphs out of reach for Subgraph GNNs? How does it perform thereon?*
- (**Q3**) *How does HyMN perform on real-world datasets w.r.t. strong GNN baselines?*
- (**Q4**) *What is the impact of incorporating CSEs?*

Synthetic experiment for counting substructures. The ability of a model to count local substructures is an acknowledged way of evaluating its expressive power (Bouritsas et al., 2022; Arvind et al., 2020; Tahmasebi et al., 2020). In order to answer (**Q1**) and test the efficacy of subgraph sampling with node centrality, we explored the ability of a Subgraph GNN to (learn to) count different small substructures as we increase the number of subgraphs in our bag. We closely followed the experimental procedure of (Chen et al., 2020), but modified the data generation process to render the task more challenging and informative[5]. We compared the performance of sampling subgraphs based on different approaches: random sampling and sampling based on the highest values of different centrality measures. No CSEs are employed in this setting. We remark that this experiment is intrinsically different than what explored in Section 3.2. There, we studied the correlation between subgraph counts and marking-induced perturbations on untrained models; here, we *train* models to *regress* these values (potentially making use of the additionally provided marking information). Figure 3 reports results for triangle counting, expressed in terms of Test Mean Absolute Error (MAE). These results demonstrate the significant improvement afforded by high-centrality sampling over random sampling with fewer subgraphs (**Q1**). Additionally, it shows that SC-based sampling generally outperformed other centrality measures, demonstrating the benefits of focusing on walk-based centralities, in alignment with our analysis in Section 3. The full set of results for additional substructures is reported in Appendix F.

Table 2: Results on OGB datasets (Test ROC-AUC). The first and second best results for each task are color-coded. Symbol '-' indicates the method is not (found to have been) benchmarked on the specific dataset.

	Method	MOLHIV	MOLBACE	MOLTOX21
	GCN	76.06 ±0.97	79.15 ±1.44	75.29 ±0.69
	GIN	75.58 ±1.40	72.97 ±4.00	74.91 ±0.51
	FULL	76.54 ±1.37	78.41 ±1.94	76.25 ±1.12
Subsampled Subgraph GNNs	OSAN (T = 10)	-	76.30 ±3.00	-
	MAG-GNN (T = 2)	77.12 ±1.13	-	-
	RANDOM (T = 2)	77.55 ±1.24	75.36 ±4.28	76.65 ±0.89
	CS-GNN (T = 2)	77.72 ±0.76	80.58 ±1.04	-
	POLICY-LEARN (T = 2)	79.13 ±0.60	78.40 ±2.85	77.47 ±0.82
	HyMN (GIN, T=2) no CSE	79.77 ±0.70	78.22 ±4.02	**77.68** ±0.71
	HyMN (GIN, T=2)	**81.01** ±1.17	**81.16** ±1.21	77.30 ±0.35
	RANDOM (T=5)	77.30 ±2.56	78.14 ±2.36	76.62 ±0.89
	CS-GNN (T = 5)	79.09 ±0.90	79.64 ±1.43	-
	POLICY-LEARN (T=5)	78.49 ±1.01	78.39 ±2.28	77.36 ±0.60
	HyMN (GIN, T=5) no CSE	79.62 ±1.14	78.57 ±1.31	**77.82** ±0.59
	HyMN (GIN, T=5)	**80.17** ±1.40	**80.64** ±0.48	76.99 ±0.45

OGB. We tested HyMN on several datasets for graph property prediction from the OGB benchmark (Hu et al., 2020b). We focus, in particular, on molecular graphs, tasked to predict global properties such as their toxicity or their ability

[4] Code to reproduce experimental results is available at https://github.com/jks17/HyMN/.

[5] In particular, we considered larger graphs with a similar number of nodes to correct an undesired correlation between the graph size and the task targets observed in the original data (see Appendix G.2).

Method	Precomp. (s)	Train (s/epoch)	Test (s)	Pept.-Func (↑)	Pept.-Struct (↓)
GIN	0.00 ±0.00	2.65 ±0.01	0.238 ±0.004	0.6555 ±0.0088	0.2497 ±0.0012
GIN + CSE	20.12 ±0.39	2.78 ±0.01	0.253 ±0.004	0.6619 ±0.0077	0.2479 ±0.0011
HyMN (GIN, T=1)	23.71 ±0.34	4.93 ±0.03	0.420 ±0.002	0.6857 ±0.0055	0.2464 ±0.0013
HyMN (GIN, T=2)	23.75 ±0.32	6.60 ±0.03	0.561 ±0.001	0.6863 ±0.0050	**0.2457** ±0.0012
GCN	0.00 ±0.00	2.07 ±0.04	0.234 ±0.006	0.6739 ±0.0024	0.2505 ±0.0023
GCN + CSE	20.19 ±0.36	2.16 ±0.04	0.254 ±0.005	0.6812 ±0.0037	0.2499 ±0.0010
HyMN (GCN, T=1)	23.88 ±0.30	2.94 ±0.01	0.292 ±0.002	**0.6912** ±0.0170	0.2481 ±0.0013
HyMN (GCN, T=2)	23.97 ±0.30	3.83 ±0.01	0.368 ±0.002	**0.6948** ±0.0052	0.2477 ±0.0010
GPS	20.87 ±0.43	8.39 ±0.05	0.611 ±0.005	0.6535 ±0.0041	0.2500 ±0.0005
Graph-ViT	29.12 ±0.61	6.78 ±0.01	0.709 ±0.009	**0.6942** ±0.0075	**0.2449** ±0.0016
G-MLP-Mixer	29.52 ±0.69	6.87 ±0.03	0.684 ±0.003	**0.6921** ±0.0054	0.2475 ±0.0015

Table 3: Results on Peptides datasets with timing comparisons on Peptides-Func using a NVIDIA GeForce RTX 3080 10GB. Test AP is quoted for Peptides-Func and Test MAE for Peptides-Struct.

Method	Train (s/epoch)	Test (s)	MalNet-T. (↑)
GIN	7.16 ±0.04	0.70 ±0.03	91.10 ±0.98
HyMN (T=1) no CSE	8.79 ±0.01	0.94 ±0.01	**92.84** ±0.52
HyMN (T=1)	9.31 ±0.02	1.02 ±0.01	**92.54** ±0.75
HyMN (T=2) no CSE	11.71 ±0.17	1.38 ±0.01	92.18 ±0.64
HyMN (T=2)	11.97 ±0.06	1.40 ±0.02	**92.44** ±0.35
GPS (Perf.)	59.34 ±0.52	6.43 ±0.02	92.14 ±0.24
GPS (BigBird)	112.63 ±1.26	17.65 ±0.05	91.02 ±0.48
GPS (Transf.)*	162.10 ±1.37	14.97 ±0.04	90.85 ±0.68

Table 4: Results and timing comparisons using a GeForce RTX 2080 8 GB for the MalNet-Tiny dataset. The model marked with * did not fit in memory with batch size 16, and was trained with batch size 4. Both HyMN and GPS employ a GIN backbone.

to inhibit HIV replication. To further examine (**Q1**), Table 2 shows the performance of our approach in relation to MPNNs, a full-bag Subgraph GNN and other subgraph sampling policies with the same number of subgraphs. Notably, even without using the centrality-based encoding (HyMN w/out CSE), our method matches the performance of a learnable sampling policy (POLICY-LEARN (Bevilacqua et al., 2024)) and consistently outperforms MPNNs and random sampling policies. Additionally, we observe that augmenting node features with CSEs can significantly increase performance on MOLHIV and MOLBACE, outperforming a full-bag Subgraph GNN (**Q4**). These results suggest that centrality sampling is effective and that additionally incorporating centrality information can lead to performance improvements on real-world datasets, aligning with our findings in Section 3. We last highlight the exceptional result HyMN obtains, with $T = 2$, on the MOLHIV benchmark (81.01 ± 1.17). This model outperforms strong GNN baselines, as reported in Appendix F.2, Table 8 (**Q3**). Run-time comparisons for this dataset are additionally enclosed in Appendix H.

Peptides. In order to evaluate the ability of HyMN to scale to larger graphs (**Q2**), we experimented on the Peptides datasets from the LRGB benchmark (Dwivedi et al., 2022), where the task is to predict global structural and functional properties of peptides, represented as graphs. The average number of nodes in these graphs is 150.94, so it is difficult for a full-bag Subgraph GNN to process. Additionally, using the centrality encoding to sample just one or two additional node-marked subgraphs can improve performance on both datasets. We also outperform GPS (Rampášek et al., 2022) (a Graph Transformer) and match the performance of Graph-MLP-Mixer (He et al., 2023) (**Q3**). Our timing experiments on Peptides-Func demonstrate that we are significantly more efficient than both of these approaches, only increasing the training time per epoch over a GCN by 42% and the inference time by 25% using 'HyMN (GCN, T=1)' (**Q2**).

MalNet-Tiny. This is a *code* dataset consisting of function call graphs with up to 5,000 nodes (Freitas et al., 2021). Models are asked to predict their malware class, or identify them as benign otherwise. As well as being from a significantly different domain, these graphs are considerably larger than the graph benchmarks considered above, allowing us to showcase *HyMN's ability to scale to even larger graphs* (**Q2**). We compare to the GPS architecture (Rampášek et al., 2022), instantiated with various (sparse) variations of its Graph Transformer component and a GIN message-passing backbone, the same we employ for HyMN. The results are shown in Table 4. Whilst, full-bag Subgraph Graph Neural Networks cannot scale to this dataset, our method, HyMN, is able to outperform sparse Transformer-based approaches at a fraction of the runtime: our approach is, *almost six times* faster than the best GPS variant both in training and inference.

Reddit. To further showcase the ability of HyMN to scale to large graphs and to evaluate the effectiveness of the method with a different data modality, we experimented with the REDDIT-BINARY (RDT-B) dataset (Morris et al., 2020a). The task involves the classification of social networks that have a high average number of nodes (429), so full-bag approaches cannot be applied. We compare our approach with a learnable sampling policy (POLICY-LEARN (Bevilacqua et al., 2024)) and to two expressive higher order GNNs (SIN and CIN) (Bodnar et al., 2021a;b). HyMN exhibits on-par performance with the best-performing method (5) which is a learnable policy, highlighting the effectiveness of our sampling approach.

Summary. In reference to the questions enlisted above, we conclude the following. (**A1**) The results from substructure counting and on the OGB benchmarks suggest a positive answer to **Q1**: SC-based sampling significantly outperformed random sampling on both, and matched the performance of the learnable POLICY-LEARN. (**A2**) HyMN was effortlessly applied to the larger Peptides and MalNet datasets, with strong empirical performance and extremely lightweight inference and training run-times. This demon-

Table 5: Results on RDT-B (Accuracy).

Method	RDT-B
GIN	92.4 ±2.5
SIN	92.2 ±1.0
CIN	92.4 ±2.1
FULL	OOM
RANDOM (T=20)	92.6 ±1.5
RANDOM (T=2)	92.4 ±1.0
POLICY-LEARN (T=2)	93.0 ±0.9
HyMN (T=2)	93.2 ±2.2

strates that effective subgraph sampling unlocks the applicability of Subgraph GNNs to larger graphs, even orders of magnitude larger than those full-bag methods could possibly be applied to. (**A3**) Beyond these two datasets, HyMN also attained remarkable performance on OGB benchmarks, and performed competitively on ZINC (see Appendix F.2). This suggests a positive answer to **Q3**. (**A4**) We observe that CSEs can enhance the performance of standard MPNNs (see Table 3) and subsampled Subgraph GNNs (see, e.g., MOLHIV and MOLBACE in Table 2). We note, however, they were not always beneficial (see MOLTOX21 Table 2 and MalNet Table 4).

6. Conclusions

We introduced a novel Subgraph GNN method, termed HyMN, which strikes a compelling balance between efficiency and expressiveness by combining a subgraph sampling strategy and structural encodings both derived from walk-based centrality measures. HyMN attains strong empirical performance with an extremely thin computational overhead, making it applicable to a wide spectrum of downstream tasks featuring large graphs, even tens or hundreds of times larger than those full-bag Subgraph GNNs can possibly process. In our paper, we showed, in particular, that the Subgraph Centrality by Estrada & Rodriguez-Velazquez (2005) is a good measure of subgraph importance: for a very limited number of subgraphs it enables competitive performance and outperforms random and learnable selection strategies. We also proved that the additional inclusion of centrality-based SEs is beneficial both theoretically and in practice, allowing to enhance discriminative power and downstream generalization performance on several real-world benchmarks.

Limitations and future work. Our sampling procedure does not take into account already sampled subgraphs unlike methods such as the ones in (Zhao et al., 2022; Bevilacqua et al., 2024). Future work could focus on more general perturbation analyses to give an indication on multi-node marking for higher-order selection policies (Qian et al., 2022) or to *quantify* (i) the optimality of the designed sampling strategy, (ii) the impact of adding subgraphs to a partially populated bag. More sophisticated selection strategies could combine different walk-based centrality measures or consider pairwise structural features.

Acknowledgments

The authors would like to thank Giorgos Bouritsas for insightful early-stage discussions and Moshe Eliasof for late stage experimental insights on PolicyLearn. J.S. is supported by the UKRI CDT in AI for Healthcare http://ai4health.io (EP/S023283/1). Y.E. is supported by the Zeff PhD Fellowship; G.B.S. by the Jacobs Qualcomm PhD Fellowship. M.B. is supported by EPSRC Turing AI World-Leading Research Fellowship No. EP/X040062/1 and EPSRC AI Hub on Mathematical Foundations of Intelligence: An "Erlangen Programme" for AI No. EP/Y028872/1. H.M. is a Robert J. Shillman Fellow and is supported by the Israel Science Foundation through a personal grant (ISF 264/23) and an equipment grant (ISF 532/23). F.F. conducted this work supported by an Andrew and Erna Finci Viterbi and, partly, by an Aly Kaufman Post-Doctoral Fellowship. F.F. partly performed this work while visiting the Machine Learning Research Unit at TU Wien led by Prof. Thomas Gärtner.

Impact Statement

This paper presents work whose goal is to advance the field of Machine Learning. There are many potential societal consequences of our work, none which we feel must be specifically highlighted here.

References

Abboud, R., Ceylan, İ. İ., Grohe, M., and Lukasiewicz, T. The surprising power of graph neural networks with random node initialization. In *Proceedings of the Thirtieth International Joint Conference on Artifical Intelligence (IJCAI)*, 2021.

Arvind, V., Fuhlbrück, F., Köbler, J., and Verbitsky, O. On Weisfeiler-Leman invariance: Subgraph counts and related graph properties. *Journal of Computer and System Sciences*, 113:42–59, 2020.

Bar-Shalom, G., Bevilacqua, B., and Maron, H. Subgraphormer: Unifying subgraph gnns and graph transformers via graph products. In *Forty-first International Conference on Machine Learning*, 2024a.

Bar-Shalom, G., Eitan, Y., Frasca, F., and Maron, H. A flexible, equivariant framework for subgraph gnns via graph products and graph coarsening. In Globerson, A., Mackey, L., Belgrave, D., Fan, A., Paquet, U., Tomczak, J., and Zhang, C. (eds.), *Advances in Neural Information Processing Systems*, volume 37, pp. 101168–101222. Curran Associates, Inc., 2024b.

Benzi, M. and Klymko, C. Total communicability as a centrality measure. *Journal of Complex Networks*, 1(2): 124–149, 2013.

Benzi, M. and Klymko, C. A matrix analysis of different centrality measures. *arXiv preprint arXiv:1312.6722*, 2014.

Bevilacqua, B., Frasca, F., Lim, D., Srinivasan, B., Cai, C., Balamurugan, G., Bronstein, M. M., and Maron, H. Equivariant subgraph aggregation networks. In *International Conference on Learning Representations*, 2021.

Bevilacqua, B., Eliasof, M., Meirom, E., Ribeiro, B., and Maron, H. Efficient subgraph gnns by learning effective selection policies. In *The Twelfth International Conference on Learning Representations*, 2024.

Biewald, L. et al. Experiment tracking with weights and biases, 2020.

Bodnar, C., Frasca, F., Otter, N., Wang, Y., Lio, P., Montufar, G. F., and Bronstein, M. Weisfeiler and lehman go cellular: Cw networks. *Advances in neural information processing systems*, 34:2625–2640, 2021a.

Bodnar, C., Frasca, F., Wang, Y., Otter, N., Montufar, G. F., Lio, P., and Bronstein, M. Weisfeiler and lehman go topological: Message passing simplicial networks. In *International Conference on Machine Learning*, pp. 1026–1037. PMLR, 2021b.

Bouritsas, G., Frasca, F., Zafeiriou, S. P., and Bronstein, M. Improving graph neural network expressivity via subgraph isomorphism counting. *IEEE Transactions on Pattern Analysis and Machine Intelligence*, 2022.

Bresson, X. and Laurent, T. Residual gated graph convnets. *arXiv preprint arXiv:1711.07553*, 2017.

Brouwer, A. E. and Spence, E. Cospectral graphs on 12 vertices. *the electronic journal of combinatorics*, pp. N20–N20, 2009.

Chen, Z., Chen, L., Villar, S., and Bruna, J. Can graph neural networks count substructures? *Advances in neural information processing systems*, 33:10383–10395, 2020.

Chuang, C.-Y. and Jegelka, S. Tree mover's distance: Bridging graph metrics and stability of graph neural networks. *Advances in Neural Information Processing Systems*, 35: 2944–2957, 2022.

Cotta, L., Morris, C., and Ribeiro, B. Reconstruction for powerful graph representations. *Advances in Neural Information Processing Systems*, 34:1713–1726, 2021.

Cybenko, G. Approximation by superpositions of a sigmoidal function. *Mathematics of control, signals and systems*, 2(4):303–314, 1989.

Dupty, M. H. and Lee, W. S. Graph representation learning with individualization and refinement. *arXiv preprint arXiv:2203.09141*, 2022.

Dwivedi, V. P. and Bresson, X. A generalization of transformer networks to graphs. *AAAI Workshop on Deep Learning on Graphs: Methods and Applications*, 2021.

Dwivedi, V. P., Luu, A. T., Laurent, T., Bengio, Y., and Bresson, X. Graph neural networks with learnable structural and positional representations. In *International Conference on Learning Representations*, 2021.

Dwivedi, V. P., Rampášek, L., Galkin, M., Parviz, A., Wolf, G., Luu, A. T., and Beaini, D. Long range graph benchmark. *Advances in Neural Information Processing Systems*, 35:22326–22340, 2022.

Dwivedi, V. P., Joshi, C. K., Luu, A. T., Laurent, T., Bengio, Y., and Bresson, X. Benchmarking graph neural networks. *Journal of Machine Learning Research*, 24 (43):1–48, 2023.

Estrada, E. and Rodriguez-Velazquez, J. A. Subgraph centrality in complex networks. *Physical Review E*, 71(5): 056103, 2005.

Fesser, L. and Weber, M. Effective structural encodings via local curvature profiles. In *The Twelfth International Conference on Learning Representations*, 2024.

Fey, M. and Lenssen, J. E. Fast graph representation learning with pytorch geometric. *ICLR 2019 Workshop on Representation Learning on Graphs and Manifolds*, 2019.

Frasca, F., Bevilacqua, B., Bronstein, M., and Maron, H. Understanding and extending subgraph gnns by rethinking their symmetries. *Advances in Neural Information Processing Systems*, 35:31376–31390, 2022.

Freeman, L. C. A set of measures of centrality based on betweenness. *Sociometry*, pp. 35–41, 1977.

Freitas, S., Dong, Y., Neil, J., and Chau, D. H. A large-scale database for graph representation learning. In Vanschoren, J. and Yeung, S. (eds.), *Proceedings of the Neural Information Processing Systems Track on Datasets and Benchmarks*, volume 1, 2021.

Geerts, F. and Reutter, J. L. Expressiveness and approximation properties of graph neural networks. In *International Conference on Learning Representations*, 2023.

Gilmer, J., Schoenholz, S. S., Riley, P. F., Vinyals, O., and Dahl, G. E. Neural message passing for quantum chemistry. In *International conference on machine learning*, pp. 1263–1272. PMLR, 2017.

Gómez-Bombarelli, R., Wei, J. N., Duvenaud, D., Hernández-Lobato, J. M., Sánchez-Lengeling, B., Sheberla, D., Aguilera-Iparraguirre, J., Hirzel, T. D., Adams, R. P., and Aspuru-Guzik, A. Automatic chemical design using a data-driven continuous representation of molecules. *ACS central science*, 4(2):268–276, 2018.

Gori, M., Monfardini, G., and Scarselli, F. A new model for learning in graph domains. In *Proceedings. 2005 IEEE International Joint Conference on Neural Networks, 2005.*, volume 2, pp. 729–734 vol. 2, 2005. doi: 10.1109/IJCNN.2005.1555942.

Hagberg, A., Swart, P. J., and Schult, D. A. Exploring network structure, dynamics, and function using networkx. Technical report, Los Alamos National Laboratory (LANL), Los Alamos, NM (United States), 2008.

He, X., Hooi, B., Laurent, T., Perold, A., LeCun, Y., and Bresson, X. A generalization of vit/mlp-mixer to graphs. In *International Conference on Machine Learning*, pp. 12724–12745. PMLR, 2023.

Hornik, K. Approximation capabilities of multilayer feedforward networks. *Neural networks*, 4(2):251–257, 1991.

Hu, S., Xiong, Z., Qu, M., Yuan, X., Côté, M.-A., Liu, Z., and Tang, J. Graph policy network for transferable active learning on graphs. *Advances in Neural Information Processing Systems*, 33:10174–10185, 2020a.

Hu, W., Fey, M., Zitnik, M., Dong, Y., Ren, H., Liu, B., Catasta, M., and Leskovec, J. Open graph benchmark: Datasets for machine learning on graphs. *Advances in neural information processing systems*, 33:22118–22133, 2020b.

Hu, W., Liu, B., Gomes, J., Zitnik, M., Liang, P., Pande, V., and Leskovec, J. Strategies for pre-training graph neural networks. In *International Conference on Learning Representations*, 2020c.

Huang, Y., Peng, X., Ma, J., and Zhang, M. Boosting the cycle counting power of graph neural networks with I^2-gnns. In *The Eleventh International Conference on Learning Representations*, 2023.

Kanatsoulis, C. and Ribeiro, A. Counting graph substructures with graph neural networks. In *The Twelfth International Conference on Learning Representations*, 2024.

Katz, L. A new status index derived from sociometric analysis. *Psychometrika*, 18(1):39–43, 1953.

Kipf, T. N. and Welling, M. Semi-supervised classification with graph convolutional networks. In *International Conference on Learning Representations*, 2017.

Kong, L., Feng, J., Liu, H., Tao, D., Chen, Y., and Zhang, M. Mag-gnn: Reinforcement learning boosted graph neural network. *Advances in Neural Information Processing Systems*, 36, 2024.

Kreuzer, D., Beaini, D., Hamilton, W., Létourneau, V., and Tossou, P. Rethinking graph transformers with spectral attention. *Advances in Neural Information Processing Systems*, 34:21618–21629, 2021.

Li, P., Wang, Y., Wang, H., and Leskovec, J. Distance encoding: Design provably more powerful neural networks for graph representation learning. *Advances in Neural Information Processing Systems*, 33:4465–4478, 2020.

Lim, D., Robinson, J. D., Zhao, L., Smidt, T., Sra, S., Maron, H., and Jegelka, S. Sign and basis invariant networks for spectral graph representation learning. In *The Eleventh International Conference on Learning Representations*, 2023.

Lim, D., Robinson, J., Jegelka, S., and Maron, H. Expressive sign equivariant networks for spectral geometric learning. *Advances in Neural Information Processing Systems*, 36, 2024.

Loshchilov, I. and Hutter, F. Decoupled weight decay regularization. In *International Conference on Learning Representations*, 2019.

Maron, H., Ben-Hamu, H., Shamir, N., and Lipman, Y. Invariant and equivariant graph networks. In *International Conference on Learning Representations*, 2018.

Micheli, A. Neural network for graphs: A contextual constructive approach. *IEEE Transactions on Neural Networks*, 20(3):498–511, 2009. doi: 10.1109/TNN.2008.2010350.

Morris, C., Ritzert, M., Fey, M., Hamilton, W. L., Lenssen, J. E., Rattan, G., and Grohe, M. Weisfeiler and leman go neural: Higher-order graph neural networks. In *Proceedings of the AAAI conference on artificial intelligence*, volume 33, pp. 4602–4609, 2019.

Morris, C., Kriege, N. M., Bause, F., Kersting, K., Mutzel, P., and Neumann, M. Tudataset: A collection of benchmark datasets for learning with graphs. In *ICML 2020 Workshop on Graph Representation Learning and Beyond (GRL+ 2020)*, 2020a.

Morris, C., Rattan, G., and Mutzel, P. Weisfeiler and leman go sparse: Towards scalable higher-order graph embeddings. *Advances in Neural Information Processing Systems*, 33:21824–21840, 2020b.

Morris, C., Lipman, Y., Maron, H., Rieck, B., Kriege, N. M., Grohe, M., Fey, M., and Borgwardt, K. Weisfeiler and leman go machine learning: The story so far. *The Journal of Machine Learning Research*, 24(1):15865–15923, 2023.

Papp, P. A. and Wattenhofer, R. A theoretical comparison of graph neural network extensions. In *International Conference on Machine Learning*, pp. 17323–17345. PMLR, 2022.

Papp, P. A., Martinkus, K., Faber, L., and Wattenhofer, R. Dropgnn: Random dropouts increase the expressiveness of graph neural networks. *Advances in Neural Information Processing Systems*, 34:21997–22009, 2021.

Paszke, A., Gross, S., Massa, F., Lerer, A., Bradbury, J., Chanan, G., Killeen, T., Lin, Z., Gimelshein, N., Antiga, L., et al. Pytorch: An imperative style, high-performance deep learning library. *Advances in neural information processing systems*, 32, 2019.

Qian, C., Rattan, G., Geerts, F., Niepert, M., and Morris, C. Ordered subgraph aggregation networks. *Advances in Neural Information Processing Systems*, 35:21030–21045, 2022.

Rampášek, L., Galkin, M., Dwivedi, V. P., Luu, A. T., Wolf, G., and Beaini, D. Recipe for a general, powerful, scalable graph transformer. *Advances in Neural Information Processing Systems*, 35:14501–14515, 2022.

Read, R. C. and Wilson, R. J. *An atlas of graphs*. Oxford University Press, 1998.

Sato, R., Yamada, M., and Kashima, H. Random features strengthen graph neural networks. In *Proceedings of the 2021 SIAM international conference on data mining (SDM)*, pp. 333–341. SIAM, 2021.

Scarselli, F., Gori, M., Tsoi, A. C., Hagenbuchner, M., and Monfardini, G. The graph neural network model. *IEEE Transactions on Neural Networks*, 20(1):61–80, 2009. doi: 10.1109/TNN.2008.2005605.

Sterling, T. and Irwin, J. J. Zinc 15–ligand discovery for everyone. *Journal of chemical information and modeling*, 55(11):2324–2337, 2015.

Sun, Q., Li, J., Peng, H., Wu, J., Ning, Y., Yu, P. S., and He, L. Sugar: Subgraph neural network with reinforcement pooling and self-supervised mutual information mechanism. In *Proceedings of the web conference 2021*, pp. 2081–2091, 2021.

Tahmasebi, B., Lim, D., and Jegelka, S. Counting substructures with higher-order graph neural networks: Possibility and impossibility results. *arXiv:2012.03174*, 2020.

Tönshoff, J., Ritzert, M., Rosenbluth, E., and Grohe, M. Where did the gap go? reassessing the long-range graph benchmark. In *The Second Learning on Graphs Conference*, 2023.

Vignac, C., Loukas, A., and Frossard, P. Building powerful and equivariant graph neural networks with structural message-passing. *Advances in neural information processing systems*, 33:14143–14155, 2020.

Wang, H., Yin, H., Zhang, M., and Li, P. Equivariant and stable positional encoding for more powerful graph neural networks. In *International Conference on Learning Representations*, 2022.

Weisfeiler, B. and Leman, A. The reduction of a graph to canonical form and the algebra which appears therein. *nti, Series*, 2(9):12–16, 1968.

Xu, K., Hu, W., Leskovec, J., and Jegelka, S. How powerful are graph neural networks? In *International Conference on Learning Representations*, 2018.

Ying, C., Cai, T., Luo, S., Zheng, S., Ke, G., He, D., Shen, Y., and Liu, T.-Y. Do transformers really perform badly for graph representation? *Advances in Neural Information Processing Systems*, 34:28877–28888, 2021.

You, J., Gomes-Selman, J. M., Ying, R., and Leskovec, J. Identity-aware graph neural networks. In *Proceedings of the AAAI conference on artificial intelligence*, volume 35, pp. 10737–10745, 2021.

Yun, C., Sra, S., and Jadbabaie, A. Small relu networks are powerful memorizers: a tight analysis of memorization capacity. *Advances in Neural Information Processing Systems*, 32, 2019.

Zhang, B., Feng, G., Du, Y., He, D., and Wang, L. A complete expressiveness hierarchy for subgraph gnns via subgraph weisfeiler-lehman tests. In *International Conference on Machine Learning*, pp. 41019–41077. PMLR, 2023a.

Zhang, B., Luo, S., Wang, L., and He, D. Rethinking the expressive power of gnns via graph biconnectivity. In *The Eleventh International Conference on Learning Representations*, 2023b.

Zhang, M. and Li, P. Nested graph neural networks. *Advances in Neural Information Processing Systems*, 34: 15734–15747, 2021.

Zhao, L., Jin, W., Akoglu, L., and Shah, N. From stars to subgraphs: Uplifting any gnn with local structure awareness. In *International Conference on Learning Representations*, 2022.

A. Outline of the Appendix Corpus

The appendix corpus is structured as follows:

- Appendix B: we include an extended background section on Subgraph GNNs, their computational complexity and bag sampling approaches to scale these architectures. This section is intended to be complementary to Section 2, as it provides additional context to readers not necessarily familiar with Subgraph GNNs and complexity limitations;
- Appendix C: we report a full algorithmic description of our HyMN approach;
- Appendix D: we report proofs pertaining to Section 4;
- Appendix E: we provide derivations and additional details on the perturbation analysis of Section 3;
- Appendix F: we report and discuss further, additional experiments – we additionally run HyMN on the ZINC dataset, we explore more backbone MPNN architectures, we compare Subgraph Centrality with other centrality measures and with RWSEs, and we further examine the impact of including CSEs in our model, alongside marking;
- Appendix G: we comprehensively describe our experimental settings and details, architectural choices and hyper-parameters;
- Appendix H: we enclose additional timing comparisons.

B. More on Subgraph GNNs and their Complexity

B.1. The Architectural Family of Subgraph GNNs

The term "Subgraph GNN" refers to a broad family of recent Graph Neural Networks sharing a common architectural pattern: that of modeling graphs as sets (bags) of subgraphs. Subgraphs are processed by a *backbone* GNN, possibly flanked by additional information sharing modules (Bevilacqua et al., 2021). Bags of subgraphs are formed by *selection policies*, which typically extract subgraphs by applying topological perturbations such as node- (Cotta et al., 2021; Papp et al., 2021) or edge-deletions (Bevilacqua et al., 2021), or by marking nodes (You et al., 2021; Papp & Wattenhofer, 2022).

In formulae, a Subgraph GNN f can be described as (Frasca et al., 2022):

$$f : G \mapsto \big(\mu \circ \rho \circ \mathcal{S} \circ \pi\big)(G), \tag{5}$$

where π is the selection policy; $\mathcal{S}$ applies the backbone GNN – with, potentially, information sharing components; ρ, μ are pooling and prediction modules.

Various choices for the above terms give rise to different Subgraph GNN variants (Frasca et al., 2022). For non-trivial selection policies and sufficiently expressive backbones, these exceed 1-WL discriminative power (Bevilacqua et al., 2021), thus surpassing standard message-passing networks.

The most popular selection policies are *node-based*: selected subgraphs are in a bijection with nodes in the original input graph. Prominent policies in this class include node-deletion, ego-networks and node-marking. From an expressiveness perspective, node-marking subsumes the first two policies (Papp & Wattenhofer, 2022; Zhang et al., 2023a), other than uncovering a connection between node-based Subgraph GNNs and node-individualization algorithms for graph isomorphism testing (Dupty & Lee, 2022). Node-marking constructs bags of subgraphs as:

$$\pi_{\mathsf{NM}} : G = (A, X) \mapsto \{(A, X \oplus e_1), \dots, (A, X \oplus e_n)\}, \tag{6}$$

where $e_i \in \{0,1\}^{n\times 1}$ is i-th element of the canonical basis [6] and $\oplus$ denotes concatenation across the channel dimension.

Node-based Subgraph GNNs encompass several architectures, including ID-GNNs (You et al., 2021), $(n-1)$-Reconstruction GNNs (Cotta et al., 2021), Nested GNNs (Zhang & Li, 2021), GNN-AK (Zhao et al., 2022), SUN (Frasca et al., 2022) and the maximally expressive GNN-SSWL (Zhang et al., 2023a). For 1-WL-expressive backbones, Subgraph GNNs with node-based policies are bounded in their expressive power by 3-WL (Frasca et al., 2022). Detailed, structured charting of their design space, along with fine-grained expressiveness results, are found in (Frasca et al., 2022; Zhang et al., 2023a).

[6] Elements in vector e_i are 0 except for the one in position i, which equals 1.

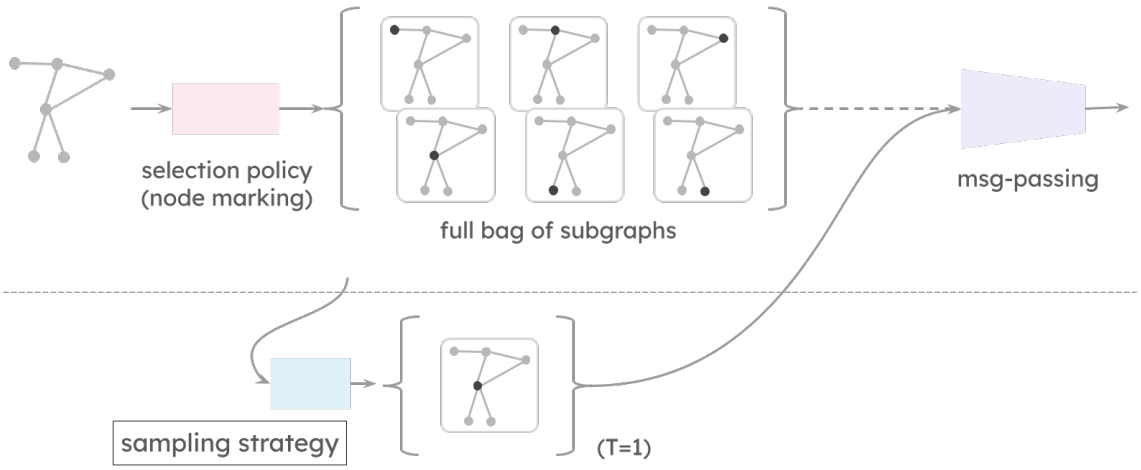

Figure 4: Depiction of a Subgraph GNN endowed with a subgraph sampling strategy.

B.2. Computational Complexity Aspects

Consider a Subgraph GNN f in the form of Equation (5), where $\mathcal{S}$ stacks neural message-passing layers. For an input graph G with n nodes and a degree bounded by d_{max}, f exhibits an asymptotic forward-pass complexity:

$$T(n, d_{\mathsf{max}}, m) = \mathcal{O}(m \cdot \overbrace{n \cdot d_{\mathsf{max}}}^{\text{msg-pass complexity}}), \tag{7}$$

with m being the number of subgraphs generated by policy π executed on graph G.

Node-based policies are such that the number of subgraphs equals the number of nodes in the original input graph, i.e., $m = n$. Hence, the complexity of node-based Subgraph GNNs scales as:

$$T(n, d_{\mathsf{max}}) = \mathcal{O}(n^2 \cdot d_{\mathsf{max}}). \tag{8}$$

Higher-order policies (Qian et al., 2022) may allow larger expressive power, but for heftier complexities. As an example, node-pair marking would induce a complexity of $\mathcal{O}(n^3 \cdot d_{\mathsf{max}})$.

The quadratic dependency on the number of nodes in Equation (8) hinders the application of Subgraph GNNs to even mildly-sized graphs. At the time of writing, experimenting on the Peptides datasets (Dwivedi et al., 2022) is already very challenging on common hardware, despite these graphs having on average ≈ 151 nodes and a similar number of edges.

B.3. Subsampling Bags of Subgraphs

To mitigate the aforementioned issue, one possibility is to reduce the number of subgraphs to process, i.e., to lower the impact of m in Equation (7). A convenient approach is to *sample* a small set k of subgraphs from the bag generated by a predefined policy π (Bevilacqua et al., 2021; Zhao et al., 2022; Bevilacqua et al., 2024; Kong et al., 2024; Sun et al., 2021) (see Figure 4). Essentially, this requires updating Equation (5) as:

$$f : G \mapsto \big(\mu \circ \rho \circ \mathcal{S} \circ \overbrace{\sigma}^{\text{sampling}} \circ \pi\big)(G). \tag{9}$$

Above, σ applies a subgraph sampling strategy to reduce the bag cardinality from m to k:

$$\sigma : B = \{G_1, \ldots, G_m\} \mapsto \tilde{B} \quad \text{s.t.} \;\; \tilde{B} \subseteq B, \;\; |\tilde{B}| = k. \tag{10}$$

The new cardinality k should scale sub-linearly in n, or be chosen as an appropriate small constant. The optimal design of strategy σ is a non-trivial task at the core of several recent works (Qian et al., 2022; Kong et al., 2024; Bevilacqua et al., 2024; Bar-Shalom et al., 2024b). In the present manuscript, we discuss a simple, effective construction based on walk-based centrality measures. Our design is justified by the theoretical considerations and empirical observations in Section 3.2, which are validated by the complementary experimental results reported in Section 5.

C. Hybrid Marking Networks in Algorithmic Form

Algorithm 1 Hybrid Marking Network

Require: Graph $G = (A, X)$, Subgraph GNN f, Max walk-length K, Number of marks T

1: $C^{\mathsf{CSE}}_{v,k} \leftarrow 0 \quad \forall v \in G, k \in [K]$ ▷ SE init.
2: $M_{v,t} \leftarrow 0 \quad \forall v \in G, t \in [T]$ ▷ Mark init.
3: $B \leftarrow I$
4: **for** $k \in [K]$ **do**
5: **for** $v \in G$ **do**
6: $C^{\mathsf{CSE}}_{v,k} \leftarrow {}^{B_{vv}}/_{k!}$ ▷ Compute SEs
7: **end for**
8: $B \leftarrow B \cdot A$
9: **end for**
10: $\tilde{C}^{SC} \leftarrow \sum_k C^{\mathsf{CSE}}_{:,k}$ ▷ Estimate SC
11: $\mathcal{M} \leftarrow$ select-top$(\tilde{C}^{SC}, T)$ ▷ Select nodes
12: **for** $t \in [T]$ **do**
13: $M_{\mathcal{M}[t],t} \leftarrow 1$ ▷ Mark nodes
14: **end for**
15: $y_G \leftarrow f(A, X \oplus C^{\mathsf{CSE}}, M)$ ▷ Forward-pass
16: **return** y_G

Algorithm 1 describes our HyMN approach, i.e., how graph representations are obtained starting from an input graph $G = (A, X)$, a backbone Subgraph GNN f, and hyper-parameters K, T[7], specifying, respectively, the maximum walk-length and the number of marks/subgraphs to select.

D. Claims and Proofs

Proposition D.1. *Let $G = (A, X)$ be a connected graph (with n nodes) with initial node features $X_i = \mathbf{p}_i^{CSE}$. There exists an $L = k + 1$ layered Message Passing Neural Network (MPNN) that processes the graph G and can compute the following structural encodings capturing closed-walk probabilities for walks of size up to k for any node i, defined as:*

$$\boldsymbol{c}_i = \left[1, \frac{(A)^1_{ii}}{\sum_{j=1}^n (A)^1_{ij}}, \frac{(A)^2_{ii}}{\sum_{j=1}^n (A)^2_{ij}}, \dots, \frac{(A)^k_{ii}}{\sum_{j=1}^n (A)^k_{ij}}\right],$$

up to arbitrary precision.

Proof. We define a Message Passing Neural Network (MPNN) as a composition of layers of the form:

$$\tilde{X}^{(l)} = AX^{(l-1)}\mathbf{W}^{(l)_1} + X^{(l-1)}\mathbf{W}^{(l)_0}, \tag{11}$$

$$X^{(l)} = f^{(l)}(\tilde{X}^{(l)}) \tag{12}$$

where $\mathbf{W}^{(l)_1}$ and $\mathbf{W}^{(l)_0}$ are learned weight matrices, and $f^{(l)}$ is an MLP for the l-th layer. We refer to the layers in Equations (11) and (12) as the MPNN layer and MLP layer, respectively, where the MLP layer is assumed to be a single hidden layer with interleaved ReLU activations.

[7]Note that, as reported in Algorithm 1, we perform a *select-top* operation (line 11). In some cases, which we found to rarely occur in practice, depending on the value of T, this operation has to arbitrarily break ties between nodes with the same exact centrality values. This tie breaking procedure can additionally be either side-stepped by marking all nodes with the same centrality value or be made equivariant by accounting for the ordering between colours from an auxiliary DS-WL-like refinement (Bevilacqua et al., 2021).

We recall that the initial node feature matrix, $X^{(0)} \in \mathbb{R}^{n\times(k+1)}$, is given as follows:

$$X^{(0)} = \begin{pmatrix} - & \mathbf{p}_1^T & - \\ - & \mathbf{p}_2^T & - \\ & \vdots & \\ - & \mathbf{p}_n^T & - \end{pmatrix}$$

where,

$$\mathbf{p}_i = \left[1, \frac{(A)_{ii}^1}{1!}, \frac{(A)_{ii}^2}{2!}, \frac{(A)_{ii}^3}{3!}, \dots, \frac{(A)_{ii}^k}{k!}\right] \in \mathbb{R}^{k+1}.$$

Step 1: Recovering the unnormalized CSE. To uncover the unnormalized CSE, we set $\mathbf{W}^{(1)_1} = 0$ and $\mathbf{W}^{(1)_0} \in \mathbb{R}^{(k+1)\times((k+1)+k)}$ as follows:

$$\mathbf{W}^{(1)_0} = \begin{pmatrix} 1 & 0 & 0 & \cdots & 0 & 0 & \cdots & 0 \\ 0 & 1! & 0 & \cdots & 0 & 0 & \cdots & 0 \\ 0 & 0 & 2! & \cdots & 0 & 0 & \cdots & 0 \\ \vdots & \vdots & \vdots & \ddots & \vdots & \vdots & \vdots & \\ 0 & 0 & 0 & \cdots & k! & 0 & \cdots & 0 \end{pmatrix}$$

Thus, the MPNN layer gives:

$$\tilde{X}^{(1)} \triangleq \text{MPNN}^{(1)}(A, X) = \begin{pmatrix} - & \mathbf{p}_1^{\text{unormalized}^T} & - \\ - & \mathbf{p}_2^{\text{unormalized}^T} & - \\ & \vdots & \\ - & \mathbf{p}_n^{\text{unormalized}^T} & - \end{pmatrix}$$

where,

$$\mathbf{p}_i^{\text{unormalized}^T} = \left[1, (A)_{ii}^1, (A)_{ii}^2, (A)_{ii}^3, \dots, (A)_{ii}^k, 0, \dots, 0\right] \in \mathbb{R}^{(k+1)+k}.$$

For the MLP f^0, we use an identity weight matrix and a bias vector, which is all zeros except for the last k values, which are ones:

$$\mathbf{b}^{(0)} = [0, 0, \dots, 0, 1, 1, \dots, 1] \in \mathbb{R}^{(k+1)+k}.$$

Thus, we obtain $X^{(1)}$, such that:

$$X_i^{(1)} = \left[1, (A)_{ii}^1, (A)_{ii}^2, (A)_{ii}^3, \dots, (A)_{ii}^k, 1, \dots, 1\right] \in \mathbb{R}^{(k+1)+k}.$$

Step 2: Compute the matrix of closed-walk probabilities. We compute the matrix of closed-walk probabilities in sequential steps. For each j-th step, we use the following weight matrices:

$$\mathbf{W}^{(j+1)_0} = \left(\begin{array}{c|c|c} I_{k+1} & 0 & 0 \\ \hline 0 & I_{j-1} & 0 \\ \hline 0 & 0 & 0_{k-(j-1)} \end{array}\right)$$

$$\mathbf{W}^{(j+1)_1} = \left(\begin{array}{c|c|c} 0_{k+1} & 0 & 0 \\ \hline 0 & 0_{j-1} & 0 \\ \hline 0 & 0 & I_{k-(j-1)} \end{array}\right)$$

Where I_n is an $n \times n$ identity matrix, and 0_n is an $n \times n$ zero matrix (if $n = 0$ the corresponding block is omitted). This means:

$$X\mathbf{W}^{(j+1)_0}$$

keeps only the first $k + j$ columns of X, and,

$$AX\mathbf{W}^{(j+1)_1}$$

multiplies by A only the last $k - (j - 1)$ columns of X.

By doing this iteratively for $j = 1$ to $j = k$, and setting the interleaved MLPs to identity weight matrices, we obtain the node matrix $\tilde{X}^{(k+1)}$, such that:

$$\tilde{X}_i^{(k+1)} = \left[1, (A)_{ii}^1, (A)_{ii}^2, (A)_{ii}^3, \ldots, (A)_{ii}^k, \sum_{j=1}^n (A)_{ij}^1, \sum_{j=1}^n (A)_{ij}^2, \ldots, \sum_{j=1}^n (A)_{ij}^k\right] \in \mathbb{R}^{(k+1)+k}.$$

Let $F : \mathbb{R}^{2k+1} \to \mathbb{R}^{k+1}$ be the following continuous function:

$$F(\mathbf{x})_i = \begin{cases} 1, \text{ if } i = 0, \\ \frac{\mathbf{x}_i}{\mathbf{x}_{k+i}}, \text{ if } i \neq 0. \end{cases}$$

Since the graph is connected, the denominator is always non-zero, making the function continuous. Additionally, since we are considering a finite graph with n nodes, the input to the function F lies within a compact set.

Using the universal approximation theorem (Hornik, 1991; Cybenko, 1989), F can be approximated to an arbitrary precision using an MLP. Thus, we use the MLP of layer $k + 1$ to realize F, obtaining the following node matrix,

$$X_i^{(k+1)} = \left[1, \frac{(A)_{ii}^1}{\sum_{j=1}^n (A)_{ij}^1}, \frac{(A)_{ii}^2}{\sum_{j=1}^n (A)_{ij}^2}, \ldots, \frac{(A)_{ii}^k}{\sum_{j=1}^n (A)_{ij}^k}\right] \in \mathbb{R}^{k+1}.$$

This completes the proof. □

Theorem D.2 (Theorem 4.1 in Section 4)**.** *There exists a pair of graphs G and G' such that for any CSE-enhanced MPNN model M_{CSE} we have $M_{CSE}(G) = M_{CSE}(G')$, but there exists a DS-Subgraph GNN model (without CSEs) $M_{sub.}$ which uses a top-k Subgraph Centrality policy such that $M_{sub.}(G) \neq M_{sub.}(G')$.*

Proof. Using the notation of (Read & Wilson, 1998), let G, G' be the quartic vertex transitive graphs Qt15 and Qt19 respectively (Here vetrex transitive means that for each pair of nodes there exists a graph automorphism that maps one node to the other, and quartic refers to 4-regular). As these graphs are 4-regular and of the same size, they are 1-WL indistinguishable. In addition, as they are vertex transitive, for each pair of indices i, j we have:

$$A_{i,i}^k = A_{j,j}^k = \frac{\text{trace}(A^k)}{12}. \tag{13}$$

$$A_{i,i}'^k = A_{j,j}'^k = \frac{\text{trace}(A'^k)}{12}. \tag{14}$$

Here the last equalities hold because both graphs have 12 vertices. Thus, to show that G and G' are indistinguishable by MPNN + centrality encoding it is enough to show that $\text{trace}(A^k) = \text{trace}(A'^k)$. As G and G' were shown in (Brouwer & Spence, 2009) to be co-spectral (i.e. their laplacian has the same eigenvalues) and 4-regular, matrices A and A' have the same eigenvalues. Thus we have:

$$\text{trace}(A)^k = \sum_{i=1}^{1} 2\lambda_i^k = \text{trace}(A')^k. \tag{15}$$

Here λ_i is the i-th eigenvalue of both A and A'. Thus the central encoding of all nodes in either graph is equal, and they are indistinguishable by any any MPNN + CE model. On the other hand, we observe that the degree histogram in the 1-hop neighborhood of any node differs between the two graphs, Qt15 and Qt19. Since an MPNN over a graph with a marked node can compute the degree distribution of the node's 1-hop neighborhood, M_{subgraph} can distinguish between the two graphs. This concludes the proof.

□

Theorem D.3 (Theorem 4.2 in Section 4)**.** *There exists a pair of graphs G and G' such that for* any *Subgraph GNN model $M_{sub.}$ which uses a top-k Subgraph Centrality policy we have $M_{sub.}(G) = M_{sub.}(G')$, but there exists an MPNN + centrality encoding model M_{CSE} such that $M_{CSE}(G) \neq M_{CSE}(G')$.*

Proof. We begin by examining the scenario where $k = 1$, meaning that our policy randomly selects subgraphs corresponding to the node with the highest centrality measure. Consider the graph G, which is formed by attaching a global node to every vertex of a cyclic graph of length 6 . Next, define G' as the graph obtained by attaching a global node to each vertex of two disconnected cyclic graphs, each of length 3 (The global node is also attached to itself through a self loop). These graphs are displayed in Figure 6. It can be easily seen that G and G' are WL indistinguishable (e.g. by induction). We first prove that both in G and G' the global node has the highest centrality measure. This implies that for both graphs, the resulting bag of subgraphs is of size one and is thus equivalent to standard message passing on the graphs (here we can ignore marking as the global nodes have a unique degree and so they can be uniquely identified by standard message passing). This implies that the two graphs are indistinguishable by any Subgraph GNN model M_{subgraph} which uses a top-1 node centrality policy. We then show that the multiset of values of the centrality encoding of each graph is different, showing that it can be distinguished by an MPNN + centrality encoding model. To show that in both graphs the global node has the higher centrality, we first prove the following lemma:

Lemma D.4. *Let A denote the adjacency graph of one of the above graphs, v denote the global node and u_1, u_2 denote a pair of nodes of the graph such that $u_1 \neq v$. For each $k \in \mathbb{N}$ we have:*

$$\begin{aligned} A^k_{v,u_2} &\geq A^k_{u_1,u_2} \\ A^k_{v,u_2} &> 0 \\ A^k_{v,v} &> A^k_{u_1,u_1}. \end{aligned} \tag{16}$$

Proof of lemma. We use induction on k. As v is connected to all nodes including itself , for $k = 1$, $A_{v,u_1} = 1$. Since, disregarding the global nodes, G, G' are simple graphs , we have $A_{u_1,u_1} = 0, A_{u_2,u_1} \leq 1$, thus the base case holds. Assuming the induction hypothesis holds for some k, we first notice that

$$A^{k+1}_{u_2,v} = A^k_{u_2,:} \cdot A_{:,v} \geq A^k_{u_2,:} \cdot A_{:,u_1} = A^{k+1}_{u_2,u_1}. \tag{17}$$

Here, $A^k_{u,:}, A^k_{:,u}$ represents the column/row vectors induced by node u respectively and $\cdot$ denotes inner product. The inequality above follows from our induction hypothesis and the fact that all entries of the matrix A^k are non-negative. Next, we notice that

$$A^{k+1}_{u_2,v} = A_{u_2,:} \cdot A^k_{:,v} \geq A_{u_2,v} \cdot A^k_{v,v} > 0. \tag{18}$$

In addition, we notice that $A^k_{v,u_1} \cdot A_{u_1,v} > 0 = A^k_{u_1,u_1} \cdot A_{u_1,u_1}$, where the last equallity holds because $A_{u_1,u_1} = 0$. Thus, we get:

$$A^{k+1}_{v,v} = A^k_{v,u_1} \cdot A_{u_1,v} + \sum_{u \neq u_1} A^k_{v,u} \cdot A_{u,v} > A^k_{u_1,u_1} \cdot A_{u_1,u_1} + \sum_{u \neq u_1} A^k_{u_1,u} \cdot A_{u,u_1} = A^{k+1}_{u_1,u_1}. \tag{19}$$

This completes the induction step. □

As explained before, the last lemma shows that top-1 centrality node marking policy always produces a bag with a single graph where the global node is marked. As the global node can be uniquely distinguished by its degree, this shows that a Subgraph GNN with this policy is equivalent to standard message passing and is thus unable to distinguish G and G'. Finally, computing the centrality encoding of order 3 we see the multiset of features of the two graphs are different and so message passing + CE is able to seperate G and G'.

We now address the general case of a top-k centrality node-marking policy. Let G_k, G'_k denote the graphs consisting of k disjoint copies of G and G', respectively. In each disjoint copy, the global node is replicated independently and maintains a higher centrality than all other nodes within that copy. Thus, in both graphs, the k nodes with the highest centrality are the k copies of the global node.

The bag of graphs generated from G_k and G'_k using the top-k centrality node-marking policy are then composed of k copies of G_k and G'_k respectively, where a single copy of the global node is marked. Notice that in each one of these bags, all graphs are isomorphic to each other, thus it is enough to show that G_k with a single marked global node copy is 1-WL indistinguishable from G'_k with a single marked global node copy. To see this holds, notice that as we have seen above, the connected component of G_k containing the marked node is 1-WL indistinguishable from the copy of the connected component of G'_k containing the marked node, and the $k - 1$ unmarked connected components of G_k are 1-WL indistinguishable from the unmarked connected components of G'_k. Thus any subgraph GNN which uses a top-k centrality

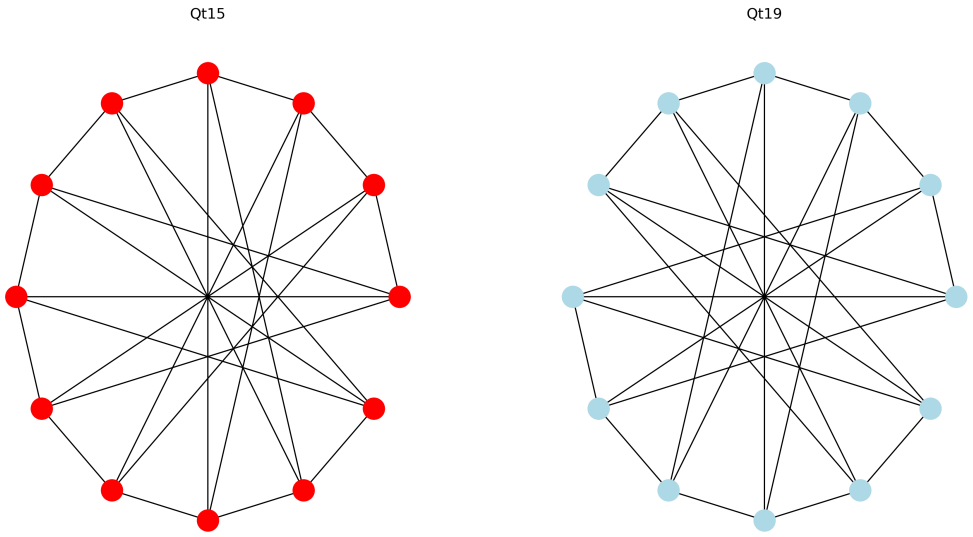

Figure 5: Two quartic vertex transitive graphs which cannot be distinguished with MPNN + CSE but can be distinguished with a Subgraph GNN with a top-1 Subgraph Centrality policy.

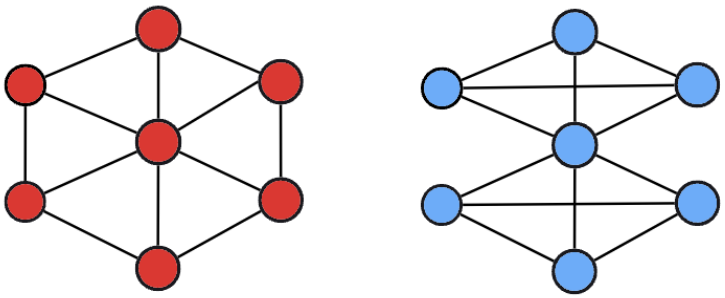

Figure 6: Two graphs which cannot be distinguished by a Subgraph GNN with a top-1 Subgraph Centrality policy without CSE but can be distinguished by an MPNN + CSE. One graph is a hexagon with a global node connected to all other nodes, and another graph which depicts two triangles connected to a global node.

node marking policy is unable to distinguish G_k and G'_k. Finally, the centrality encoding values of each node u_{copy} in G_k is equal to the centrality encoding value of the node u in G which corresponds to u_{copy}. As we have seen before the set of centrality encoding values of G and G' are different, the set of centrality encoding values of G_k and G'_k are also different, and so message passing + CE is able to separate G_k and G'_k.

□

Proposition D.5. *Let $G = (A, X)$ be a finite graph, and let $\mathcal{B}_G$ be the bag generated from original graph G. Let DSS-GNN be the subgraph-based GNN that processes the bag $\mathcal{B}_G$. There exists a set of weights for DSS-GNN, such that DSS-GNN$(\mathcal{B}_G)$ = MPNN(G) for any MPNN processing G with centrality-based structural encodings as initial node features.*

Proof. Let $\{X^i, A^i\}_{i=1}^n$ represent the node feature matrix X^i and adjacency matrix A^i, respectively, for the i-th subgraph in the collection of subgraphs. We adopt the binary node-marking technique from (Bevilacqua et al., 2021), where X^i

includes a one-hot encoded vector for the root node identification, with a 1 in the i-th position,[8]

$$X^i = \begin{pmatrix} 0 \\ \vdots \\ 0 \\ 1 \\ 0 \\ \vdots \\ 0 \end{pmatrix} \quad \text{with 1 at the } i\text{-th position,} \tag{20}$$

we note that in this case, the adjacencies of all subgraphs, denoted as $\{A^i\}_{i=1}^n$, are identical to the adjacency of the original graph, A.

We recall that the DSS-GNN architecture applies an MPNN over each subgraph independently, followed by an MLP. Subsequently, an MPNN followed by an MLP operates on a shared component, enabling information sharing across subgraphs.

To be more explicit, the architecture is defined as follows:

$$\tilde{X}^{l;i} = \text{MPNN}^{l;1}(A^i, X^{l-1;i}), \tag{21}$$

$$Y^{l-1;i} = f^{l;1}(\tilde{X}^{l-1;i}), \tag{22}$$

$$\tilde{X}^{l-1} = \text{MPNN}^{l;2}\left(\sum_{j=1}^n A^j, \sum_{j=1}^n X^{l-1;j}\right), \tag{23}$$

$$Y^{l-1} = f^{l;2}(\tilde{X}^{l-1}), \tag{24}$$

$$X^{l+1;i} = Y^{l-1;i} + Y^{l-1}, \tag{25}$$

where the MPNN is defined as:

$$\text{MPNN}(X) = AX\mathbf{W}^1 + X\mathbf{W}^0. \tag{26}$$

The proof proceeds in three steps. First, we compute the centrality encoding at the root nodes, recall Equation (4), specifically at X_i^i. Second, we use the shared information component to propagate this root node information across all subgraphs. Finally, we simulate an MPNN over each subgraph. Since the subgraphs are identical and equipped with the centrality encoding, the proof is complete.

Step 1. We begin by applying the K MPNN layers to each subgraph independently, and setting to 0 the weight matrices of the shared component, effectively enforcing no sharing between the subgraphs.

More specifically, at the k-th layer, the following weight matrices are used:

$$\mathbf{W}^0 = \begin{pmatrix} 1 & 0 & \cdots & 0 & 0 \\ 0 & 1 & \cdots & 0 & 0 \\ \vdots & \vdots & \ddots & \vdots & \vdots \\ 0 & 0 & \cdots & 1 & 0 \end{pmatrix}_{k\times(k+1)}, \quad \mathbf{W}^1 = \begin{pmatrix} 0 & 0 & \cdots & 0 & 0 \\ 0 & 0 & \cdots & 0 & 0 \\ \vdots & \vdots & \ddots & \vdots & \vdots \\ 0 & 0 & \cdots & 0 & 1 \end{pmatrix}_{k\times(k+1)}$$

where:

- $\mathbf{W}^0$ is a $k \times (k+1)$ matrix consisting of a $k \times k$ identity matrix $\mathbf{I}_k$ followed by an extra column of zeros:

$$\mathbf{W}^0 = \begin{pmatrix} \mathbf{I}_k & \mathbf{0}_{k\times 1} \end{pmatrix}$$

[8] Although this proof does not consider additional node features, it can be easily adapted to incorporate them.

Specifically, when $\mathbf{W}^0$ is multiplied by a matrix $B \in \mathbb{R}^{n\times k}$, i.e., $B\mathbf{W}^0$, it appends a column of zeros to the right of B, leaving the structure of B unchanged but with an additional column of zeros.

- $\mathbf{W}^1$ is a $k \times (k+1)$ matrix consisting of a $k \times k$ zero matrix $\mathbf{0}_{k\times k}$ followed by a column of all zeros except for a 1 in the last row:
$$\mathbf{W}^1 = \begin{pmatrix} \mathbf{0}_{k\times k} & \mathbf{e}_k \end{pmatrix}$$
Specifically, when $\mathbf{W}^1$ is multiplied by a matrix $B \in \mathbb{R}^{n\times k}$, i.e., $B\mathbf{W}^1$, the resulting matrix is composed of the zero matrix and the last column of B. In other words, this operation extracts the last column of B and appends it to a matrix of zeros of size $k \times k$.

In this setup, for each i, the term $AX^i\mathbf{W}^1$ at the k-th layer propagates the node marking to neighboring nodes and places it in the last column. Meanwhile, the term $X\mathbf{W}^0$ copies the propagated marking from the previous k layers.

Thus, by summing the two terms, after K layers, the node features X^i_j are given by:

$$X^i_j = \begin{cases} \left[1, A^1_{ii}, A^2_{ii}, \dots, A^K_{ii}\right], & \text{for } j = i, \\ \left[0, \mathbf{v}_j\right], & \text{for } j \neq i, \end{cases} \tag{27}$$

where $\mathbf{v}_j$ holds at its k-th slot the number of marks propagated to node j in subgraph i at the step k.

Since each entry in the vectors X^i_j for any $i \in [n]$ and $j \in [n]$ represents the propagation of a mark over $k \in [K]$ steps — specifically, the number of walks from the root node of subgraph i to node j (within subgraph i) — the number of possible values for these vectors is constrained. Moreover, because the original graph is finite, the total number of possible values for these vectors must also be finite.

By Theorem 3.1 in (Yun et al., 2019)[9], there exists an MLP at the K-th layer that can implement the following mappings:

$$f^k([1, a_1, a_2, \dots, a_K]) = \left[1, \frac{a_1}{1!}, \frac{a_2}{2!}, \dots, \frac{a_K}{K!}\right], \tag{28}$$
$$f^k([z, b_1, b_2, \dots, b_K]) = \mathbf{0}_{K+1}, \tag{29}$$

for any $z \neq 1$ and $a_i, b_i \in \mathbb{R}$. At this step, the root nodes i hold the centrality value, recall Equation (4), while all other nodes hold the feature vector $\mathbf{0}_{K+1}$.

Step 2. Next, we utilize the shared information component by setting the weights of its MPNN as follows, $\mathbf{W}^1 = 0$ and $\mathbf{W}^0 = I$, which effectively broadcasts the root node information to the corresponding nodes in all other subgraphs. To prevent the root nodes from receiving double the value, we initialize the MPNN that operates on each subgraph individually with zero weights.

Step 3. At this point, we have n copies of the original graph, each equipped with its corresponding centrality values. Therefore, the MPNN over each subgraph can effectively simulate the MPNN over the original graph, now with centrality values assigned to the nodes. Assuming a mean readout is used at the conclusion of both the DSS-GNN($\mathcal{B}_G$ and the MPNN(G), their outputs will be identical.

This concludes the proof.

We note that this result is also valid for Subgraph GNN architectures that subsume DSS-GNN, e.g., GNN-SSWL+ (Zhang et al., 2023a). □

E. On Marking-Induced Perturbations and the Number of Walks

In this section, we report more details and comments on our Observation 1 introduced in Section 3.2.

[9]This theorem assumes the output is bounded between -1 and 1. However, we can relax this assumption as long as the outputs are bounded (and they are since the original graph is finite). To handle this, we can use the theorem to calculate the normalize values (dividing each value by the upper bound), and then use an additional MLP to scale the results back to the original values.

We start by commenting on Equation (3). We recall that we are interested in upper-bounding the amount of output perturbation induced by marking node v. Effectively, this corresponds to the distance $|y_G - y_{S_v}|$, namely, the absolute difference between the predictions a backbone MPNN computes for the original graph (G) and the subgraph obtained by marking node v (S_v).

For an L-layer MPNN in the form of Equation (2), we obtain Equation (3) by an almost immediate application of the results in (Chuang & Jegelka, 2022). Indeed, let us rewrite:

$$|y_G - y_{S_v}| = |\phi^{(L+1)}\big(\sum_{u\in G} h_u^{G,(L)}\big) - \phi^{(L+1)}\big(\sum_{u\in S_v} h_u^{S_v,(L)}\big)| \tag{30}$$

where $h_v^{G,(L)}, h_v^{S_v,(L)}$ indicate, respectively, the representations of node u in graph G and its perturbed counterpart S_v. Now, by Chuang & Jegelka (2022, Theorem 8) we have:

$$|y_G - y_{S_v}| \leq \prod_{l=1}^{L+1} K_\phi^{(l)} \cdot \underbrace{\text{TMD}_w^{L+1}(G, S_v)}_{(\mathcal{A})} \tag{31}$$

where $(\mathcal{A})$ is the $L+1$-depth *Tree Mover's Distance* (TMD) (Chuang & Jegelka, 2022) with layer-weighting w calculated between the original graph and its marked counterpart.

In the same work, the authors provide an upper-bound on the TMD between a graph and a perturbed version obtained by a change in the initial features of a node (Chuang & Jegelka, 2022, Proposition 11). We restate this result.

Proposition E.1. *(Chuang & Jegelka, 2022, Proposition 11) Let H be a graph and H' be the perturbed version of H obtained by changing the features of node v from x_v to x'_v. Then:*

$$\textit{TMD}_w^L(H, H') \leq \sum_{l=1}^{L} \lambda_l \cdot \textit{Width}_l(T_v^L) \cdot \|x_v - x'_v\| \tag{32}$$

where $\lambda_l \in \mathbb{R}^+$ is a layer-wise weighting scheme dependent of w and $\textit{Width}_l(T_v^L)$ is the width at the l-th level of the L-deep computational tree rooted in v.

We can readily apply Proposition E.1 and leverage the fact that marking only induces a unit-norm feature perturbation to get:

$$|y_G - y_{S_v}| \leq \prod_{l=1}^{L+1} K_\phi^{(l)} \cdot \text{TMD}_w^{L+1}(G, S_v) \tag{33}$$

$$\leq \prod_{l=1}^{L+1} K_\phi^{(l)} \cdot \sum_{l=1}^{L+1} \lambda_l \cdot \text{Width}_l(T_v^{L+1}) \tag{34}$$

Finally, we note that $\text{Width}_l(T_v^{L+1})$ corresponds to the number of walks of length $l-1$ starting from v. This can be easily seen by noting that the leaves of the computational tree can be put in a bijection with all and only those walks of length $l-1$ starting from v[10]. This value is notoriously computed from row-summing powers of the adjacency matrix A, so that: $\text{Width}_l(T_v^{L+1}) = \sum_j (A^{l-1})_{v,j}$. We ultimately have:

$$|y_G - y_{S_v}| \leq \prod_{l=1}^{L+1} K_\phi^{(l)} \cdot \sum_{l=1}^{L+1} \lambda_l \cdot \text{Width}_l(T_v^{L+1}) \tag{35}$$

$$= \prod_{l=1}^{L+1} K_\phi^{(l)} \cdot \sum_{l=1}^{L+1} \lambda_l \cdot \sum_j (A^{l-1})_{v,j} \tag{36}$$

[10]This can be constructed, e.g., by associating leaf nodes to the walks (uniquely) obtained by "climbing up" the computational tree up to the root.

The above bound is easily extended to consider a closely related analysis: the impact of adding a single node-marked subgraph S to a bag formed by the original graph only. This analysis would enlighten us on the impact a single subgraph addition in the case of "augmented policies", which we use throughout our experiments in Section 5, see Appendix G.1.

In other words, we would like to bound $|y_G^{B=\{G\}} - y_G^{B=\{S,G\}}|$, where these outputs are given by Equation (45), with a base MPNN backbone as per Equation (2). We have:

$$|y_G^{B=\{G\}} - y_G^{B=\{S,G\}}| = |\phi^{(L+1)}\big(\sum_{v\in G}(h_{G,v}^{(L)} + h_{S,v}^{(L)})\big) - \phi^{(L+1)}\big(\sum_{v\in G} h_{G,v}^{(L)})\big)| \tag{37}$$

$$\leq K_\phi^{L+1} \cdot \| \sum_{v\in G}(h_{G,v}^{(L)} + h_{S,v}^{(L)}) - \sum_{v\in G} h_{G,v}^{(L)} \| \tag{38}$$

where K_ϕ^{L+1} is the Lipschitz constant of the prediction layer $\phi^{(L+1)}$. We can rewrite the above as follows by appropriately rearranging terms and by the triangular inequality:

$$|y_G^{B=\{G\}} - y_G^{B=\{S,G\}}| \leq K_\phi^{L+1} \cdot \| \sum_{v\in G}(h_{G,v}^{(L)} + h_{S,v}^{(L)}) - \sum_{v\in G} h_{G,v}^{(L)} \| \tag{39}$$

$$\leq K_\phi^{(L+1)} \cdot \Big(\| \sum_{v\in G} h_{G,v}^{(L)} \| + \underbrace{\| \sum_{v\in G} h_{S,v}^{(L)} - \sum_{v\in G} h_{G,v}^{(L)} \|}_{(\mathcal{A})} \Big) \tag{40}$$

where, we note, $(\mathcal{A})$ is the distance between the embeddings of the marked and unmarked graphs, before a final predictor is applied. This term can be bounded similar to our initial analysis for Observation 1:

$$(1) = \| \sum_{v\in G} h_{S,v}^{(L)} - \sum_{v\in G} h_{G,v}^{(L)} \| \tag{41}$$

$$\leq \prod_{l=1}^{L} K_\phi^{(l)} \cdot \underbrace{\text{TMD}_w^{L+1}(S,G)}_{(\mathcal{B})} \tag{42}$$

where $(\mathcal{B})$ can be upper-bounded, again, by Proposition E.1[11].

Putting things together:

$$|y_G^{B=\{G\}} - y_G^{B=\{S,G\}}| \leq K_\phi^{(L+1)} \cdot \Big(\| \sum_{v\in G} h_{G,v}^{(L)} \| + \prod_{l=1}^{L} K_\phi^{(l)} \cdot \sum_{l=1}^{L+1} \lambda_l \cdot \sum_j (A^{l-1})_{S,j} \Big) \tag{43}$$

Differently from the above analysis, we observe a contribution given by $\| \sum_{v\in G} h_{G,v}^{(L)} \|$. This could be upper-bounded, e.g., by the sum of the "tree-norms" Chuang & Jegelka (2022) of the computational trees over the original graph. We note that (the presence of) this term is, however, independent on the selection of the specific node to mark.

In future developments of this work we envision to more deeply enquire into the relation between Equation (43) and Equation (1), and into the principled choice of a specific centrality measure among different possibilities.

E.1. Perturbation Analysis on an Additional Dataset

As outlined in Section 3.2, we explore the amount of perturbation from different marking schemes on the output of an untrained GIN model. We have shown in Figure 1, the effect of these marking schemes on the MUTAG dataset. Here, in Figure 7a and in Figure 7b, we additionally show the results for the NCI1 dataset and for Erdös-Renyi (ER) graphs. The ER graphs are consistent with our correlation analysis experiment Section 3.2, where we randomly generate 100 ER graphs, each with $N = 20$ nodes and wiring probability $p = 0.3$.

[11] We have allowed a little abuse of notation here by using S to refer to the "subgraph" obtained by marking node S in G.

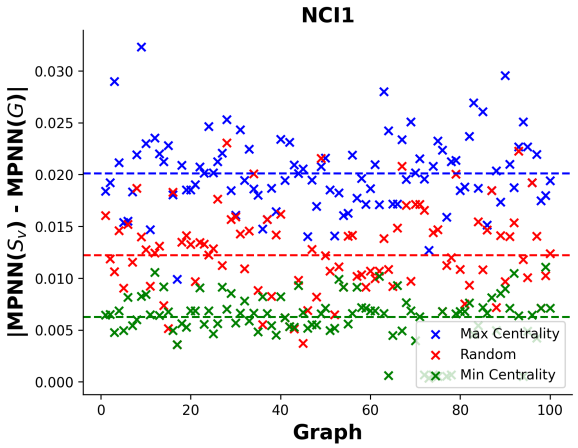

(a) NCI1 dataset alterations.

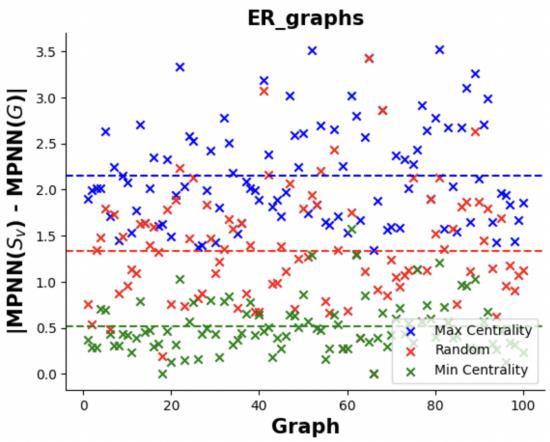

(b) Erdös-Renyi graph alterations.

Figure 7: Plots showing the alteration of graph representations using GIN by adding an additional node-marked subgraph with (i) the highest centrality, (ii) the lowest centrality, and (iii) a random marking for both the NCI1 dataset (left) and Erdös-Renyi graphs (right).

F. Additional Experiments

F.1. Additional Experiments with Other Backbones

We have already experimented with GCN as the backbone on the Peptides datasets. Additionally, we run GCN as a backbone on OGB molecular datasets (see Table 6). Interestingly, we find that a GCN backbone achieves the best results on MOLBACE. Moreover, we perform experiments on yet another backbone: GatedGCN (Bresson & Laurent, 2017). This complements backbones used in the Graph Transformer literature such as GPS. The results on peptides and MolHIV are shown in Table 7. These results further show that the walk-based centrality structural encoding can improve performance over the backbone MPNN, and we can improve performance even further by using it for sampling subgraphs.

Table 6: Results on OGB benchmarks using GCN as the backbone architecture.

Model	MolHIV	MolBace	MolTox
GCN	76.06 $\pm$0.97	79.15 $\pm$1.44	75.29 $\pm$0.69
HyMN (GCN, T=2)	76.82 $\pm$1.20	83.21 $\pm$0.51	76.07 $\pm$0.50

Table 7: Results on the Peptides and MolHIV benchmarks using GatedGCN as the backbone architecture.

Model	MolHIV	Peptides-Func	Peptides-Struct
GatedGCN	78.27 $\pm$0.65	0.6558 $\pm$0.0068	0.2497 $\pm$0.0007
GatedGCN + CSE	80.33 $\pm$0.56	0.6611 $\pm$0.0058	0.2482 $\pm$0.0010
HyMN (GatedGCN, T=2) w/out CSE	79.02 $\pm$0.91	0.6723 $\pm$0.0079	0.2473 $\pm$0.0013
HyMN (GatedGCN, T=2)	81.07 $\pm$0.21	0.6788 $\pm$0.0052	0.2471 $\pm$0.0007

F.2. Results on ZINC and Additional Model Comparisons on MolHIV

We experimented with the ZINC-12K molecular dataset (Sterling & Irwin, 2015; Gómez-Bombarelli et al., 2018), where we maintain a 500k parameter budget, in line with previous works.

We compared the test MAE using HyMN to other sampling approaches (Qian et al., 2022; Bevilacqua et al., 2024), a full-bag Subgraph GNN, a Graph Transformer (GPS) (Rampášek et al., 2022), two expressive GNN baselines (GSN, CIN) (Bouritsas et al., 2022; Bodnar et al., 2021a) and the two alternative architectures Graph-ViT and Graph MLP-Mixers by (He et al., 2023). Results are presented in Table 8. We additionally report results on MOLHIV in Table 9, often used as a reference test-bed for most full-bag methods (Bevilacqua et al., 2021; Frasca et al., 2022; Zhang & Li, 2021; Cotta et al., 2021; Zhao et al., 2022). We observe that our hybrid method can outperform full-bag Subgraph GNNs as well as previously proposed subsampling based approaches. Additionally, we perform competitively with CIN, which takes into account higher-order

Table 8: Test results on ZINC. The first and second best results are color-coded.

Method	ZINC (↓)
GCN	0.321 ±0.009
GIN	0.163 ±0.004
GSN	0.101 ±0.010
CIN	0.079 ±0.006
GPS	0.070 ±0.004
GINE-MLP-Mixer	0.073 ±0.001
GINE-ViT	0.085 ±0.004
FULL	0.087 ±0.003
OSAN	0.177 ±0.016
POLICY-LEARN (T = 2)	0.120 ±0.003
RANDOM (T = 2)	0.136 ±0.005
GIN+CSE	0.092 ±0.002
HyMN (GIN, T=1)	0.080 ±0.003
HyMN (GIN, T=2)	0.083 ±0.002

Table 9: Test results on MOLHIV. The first and second best results are color-coded.

Method	MOLHIV (↑)
GCN	76.06 ±0.97
GIN	75.58 ±1.40
Reconstr. GNN	76.32 ±1.40
DSS-GNN	76.78 ±1.66
GSN	80.39 ±0.90
CIN	80.94 ±0.57
GPS	78.80 ±1.01
GINE-MLP-Mixer	79.97 ±1.02
GINE-ViT	77.92 ±1.42
Nested-GNN	78.34 ±1.86
GNN-AK+	79.61 ±1.19
SUN	80.03 ±0.55
FULL	76.54 ±1.37
POLICY-LEARN (T = 2)	79.13 ±0.60
RANDOM (T = 2)	77.55 ±1.24
GIN+CSE	77.44 ±1.87
HyMN (GIN, T=1)	80.36 ±1.23
HyMN (GIN, T=2)	81.01 ±1.17

interactions and explicitly models ring-like structures. Non-message-passing based architectures can perform slightly better in absolute terms, but for higher run-time (see comparison with GPS in Appendix H). We highlight that additionally using subgraphs can outperform purely using the centrality-based encodings (**Q4**). In particular, the two approaches in tandem deliver exceptional performance on MolHIV, for $T = 2$.

F.3. Minimum Centrality Marking for Counting Substructures

As highlighted in Section 3.2, low-centrality nodes perturb representations only to a limited extent, causing the method to work in a regime close to a vanilla 1-WL GNN. We also empirically observe that the perturbations induced by marking high-centrality nodes correlate much more with potentially predictive features, such as subgraph counts. In order to further evidence this point, we have run experiments for counting triangle and 4-cycle substructures, studying the impact of sampling marked subgraphs associated with the minimum values of the Subgraph Centrality (SC). We report the results in Table 10 and Table 11, along with those of random sampling and max-centrality sampling (MAE, the lower the better). We observe that min-centrality sampling is indeed outperformed by the two other strategies on all settings, further suggesting the limitations of marking nodes with low subgraph centrality.

F.4. Comparison to Other Centrality Measures

We compared the impact of using different node centrality measures as a node marking scheme on how much they altered the graph representation. For each of these centrality measures, we measured the distance $\|f(S_v) - f(G)\|$ on 100 graphs from two different real-world datasets from the popular TU suite: MUTAG and NCI1 (Morris et al., 2020a). Here, f is an

Table 10: Performance comparison for different policies on triangle subgraphs.

Policy	**10 Subgraphs**	**20 Subgraphs**	**30 Subgraphs**
Min SC	0.78	0.52	0.43
Random	0.62	0.48	0.40
Max SC	0.20	0.10	0.03

Table 11: Performance comparison for different policies on 4-cycle subgraphs.

Policy	**10 Subgraphs**	**20 Subgraphs**	**30 Subgraphs**
Min SC	0.74	0.63	0.41
Random	0.59	0.45	0.36
Max SC	0.38	0.12	0.08

untrained 3-layer GIN (Xu et al., 2018). We can see from Table 12 that marking the node with using the maximum values of the three walk-based centrality measures (Subgraph, Communicability, Katz) leads to the highest average perturbation and marking the node with the minimum of these centrality measures leads to the lowest. This implies that this family of centrality measures is most aligned with the perturbation distance.

Table 12: Amount of perturbation from the original graph representation on MUTAG and NCI1 using 3-layer untrained GIN with 32 hidden dimension by incorporating a node-marked subgraph with different marking policies.

Marking Policy	MUTAG Perturbation	NCI1 Perturbation
Random	0.0648	0.0126
Minimum Degree Centrality	0.0202	0.0075
Maximum Degree Centrality	0.0968	0.0075
Minimum Closeness Centrality	0.0241	0.0073
Maximum Closeness Centrality	0.1038	0.0184
Minimum Betweenness Centrality	0.0202	0.0076
Maximum Betweenness Centrality	0.0957	0.0183
Minimum Katz Centrality	0.0177	0.0063
Maximum Katz Centrality	0.1051	0.0200
Minimum Communicability Centrality	0.0177	0.0063
Maximum Communicability Centrality	0.1056	0.0200
Minimum Subgraph Centrality	0.0177	0.0063
Maximum Subgraph Centrality	0.1055	0.0201

To further assess the benefits of our specific centrality encoding for sampling subgraphs, we compared against using other centrality measures to sample subgraphs in the counting substructure task. We used Closeness centrality, Betweeness centrality, Pagerank centrality and Degree centrality as baselines using the Networkx library (Hagberg et al., 2008). From Figure 8, we can see that using any of the different centrality methods performs better than random sampling across all substructures and number of samples. We also find that the Subgraph Centrality which we use, outperforms all other approaches in counting 3 and 4-cycles for any number of samples and in counting 3 and 4-paths when number of samples ≥ 5. For 4-cycles and other substructures, we find that Subgraph centrality is best, followed by Degree and Pagerank centrality and then Closeness and Betweenness centralities perform the worst of these centrality measures. This ranking of performance is aligned with how correlated these substructures are with the Subgaph Centrality on these synthetic graphs (as shown in Table 13).

To further compare different centrality measures, we ran additional experiments on the Peptides and MolHIV datasets. We experimented in particular, with the Betweenness Centrality (BC), the Katz Index (KI) and the Subgraph Centrality (SC). We see from Table 14 that the performances achieved by different centrality measures are not dramatically different from each other, with those by the KI and SC being closer. In fact, centrality measures often exhibit a degree of correlation with each other, especially if from the same family, as it is the case of the walk-based KI and SC (see (Estrada & Rodriguez-Velazquez, 2005) and Table 13). It is also worth noting that Subgraph Centrality can be more efficient to calculate than these other centrality measures using the Networkx library (see Table 15).

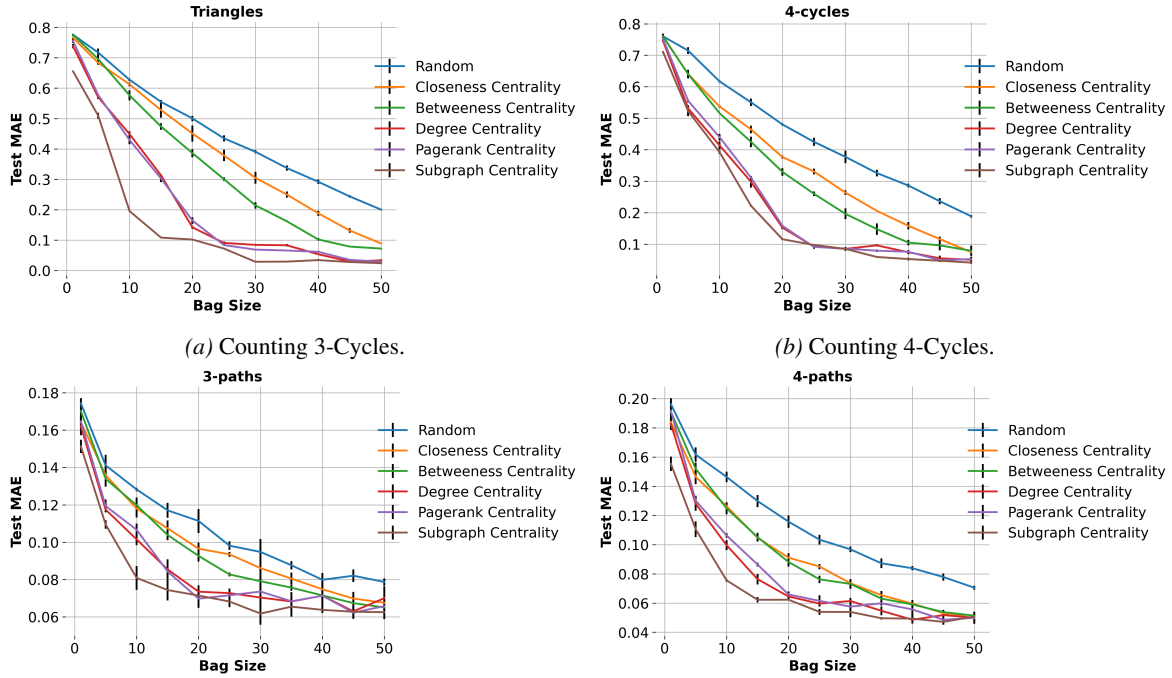

(a) Counting 3-Cycles. *(b)* Counting 4-Cycles.

(c) Counting 3-Paths. *(d)* Counting 4-paths.

Figure 8: Comparing different centrality measures for counting different substructures on synthetic random graphs.

Table 13: Correlation between the different centralities and Subgraph Centrality on the random regular graphs in the substructure counting experiments.

Centrality	Correlation with Subgraph Centrality
Pagerank Centrality	0.923 $\pm$0.025
Degree Centrality	0.970 $\pm$0.012
Betweenness Centrality	0.801 $\pm$0.074
Closeness Centrality	0.786 $\pm$0.067

Overall, we believe that specific centrality measures could work better than others depending on the task at hand, but, at the same time, our current ensemble of observations indicate that walk-based centrality measures – and, in particular, the Subgraph Centrality – offer the most competitive results for the lightest precomputation run-time. Given the additional support provided by the bound discussed in Section 3, we think they constitute particularly strong candidates across use-cases.

F.5. Comparison between Centrality-Based Structural Encodings and RWSE

Here we aim to outline some of the similarities and differences between our Centrality structural Encoding (CSE) defined in Equation (4) and the Random-Walk Structural Encoding (RWSE) introduced in (Dwivedi et al., 2021). The RWSE uses the diagonal of the k-step random-walk matrix defined in Equation (44) defined as:

$$p_i^{\text{RWSE}} = [(AD^{-1})_{ii}, (AD^{-1})^2_{ii}, \dots, (AD^{-1})^k_{ii}] \in \mathbb{R}^k, \tag{44}$$

These terms show similarity to our CSE as it also stores powers of the diagonal of the adjacency matrix, but it has a different normalization term that depends on the degree. In Proposition D.1, we show that using an MPNN with CSE can compute the the probability, for all possible walks departing from a node, that a walk will lead back to the start. RWSE structural encodings are subtly different in that they compute the landing probability of a *random* walk from a node to itself. In this case, rather than weighting all possible walks equally, the walks are weighted by the degrees of the nodes along the walk; a walk where there are fewer alternative routes (other nodes) for the RW is more likely to occur.

Here we aim to empirically examine this difference to see (i) which one is a more effective Structural Encoding and (ii)

Table 14: Comparison of different centrality measures on real-world molecular datasets.

Centrality for Sampling	MolHIV	Peptides-Func	Peptides-Struct
Betweenness Centrality	78.86 $\pm$0.98	0.6749 $\pm$0.0066	0.2478 $\pm$0.0006
Katz Index	79.58 $\pm$0.98	0.6756 $\pm$0.0056	0.2469 $\pm$0.0008
Subgraph Centrality	79.77 $\pm$0.70	0.6758 $\pm$0.0050	0.2466 $\pm$0.0010

Table 15: Timing of different centrality measures on an Erdös-Renyi graph with 1000 nodes and p=0.5 using the Networkx library.

Centrality	Time (s)
Betweenness Centrality	83.12
Katz Index	1.31
Subgraph Centrality	0.54

which one is more effective for subgraph sampling. To show the effect of both CSE and RWSE as SEs, we compared both on the Peptides datasets (Dwivedi et al., 2022) with two different base MPNNs (GCN and GIN). From Table 16, it can be seen that our centrality encoding performs similarly to the RWSE encoding; matching almost exactly except with a GCN on Peptides-Func.

To answer (ii) and highlight the benefit of sampling based on CSE over using RWSE, we compared using the sum of these different encodings to sample the subgraphs in the counting substructures experiment. From Figure 9, we see that our sampling method is better for counting all substructures and for all the number of samples in comparison to RWSE sampling.

In conclusion, Appendix G.2 shows that our CSE is better for sampling subgraphs and Table 16 shows that CSE is competitive when purely used as a Structural Encoding. Therefore, it is well motivated to use the CSE for our hybrid method where we need an SE *and* to use it as a sampling method. Future work could consider further understanding the expressivity differences between these SEs and the role of the normalization factor.

F.6. Further Examining the Effect of CSEs

In Table 2, we explore the effect of HyMN with and without CSEs. In order to complement these results, we additionally evaluated the effect of CSEs on HyMN and GIN with the Peptides and ZINC datasets. The results are reported in Table 17. These results further show that adding even one subgraph with our approach can be beneficial and that additionally using the centrality measure as a structural encoding can also improve performance.

G. Experimental Details

In this section we provide details on the experimental validation described and discussed in Section 5.

Table 16: Results on the Peptides datasets comparing CSE with RWSE.

Method	Peptides-Func (↑)	Peptides-Struct (↓)
GIN	0.6555 $\pm$0.0088	0.2497 $\pm$0.0012
GIN + RWSE	0.6621 $\pm$0.0067	0.2478 $\pm$0.0017
GIN + CSE	0.6619 $\pm$0.0077	0.2479 $\pm$0.0011
GCN	0.6739 $\pm$0.0024	0.2505 $\pm$0.0023
GCN + RWSE	0.6860 $\pm$0.0050	0.2498 $\pm$0.0015
GCN + CSE	0.6812 $\pm$0.0037	0.2499 $\pm$0.0010

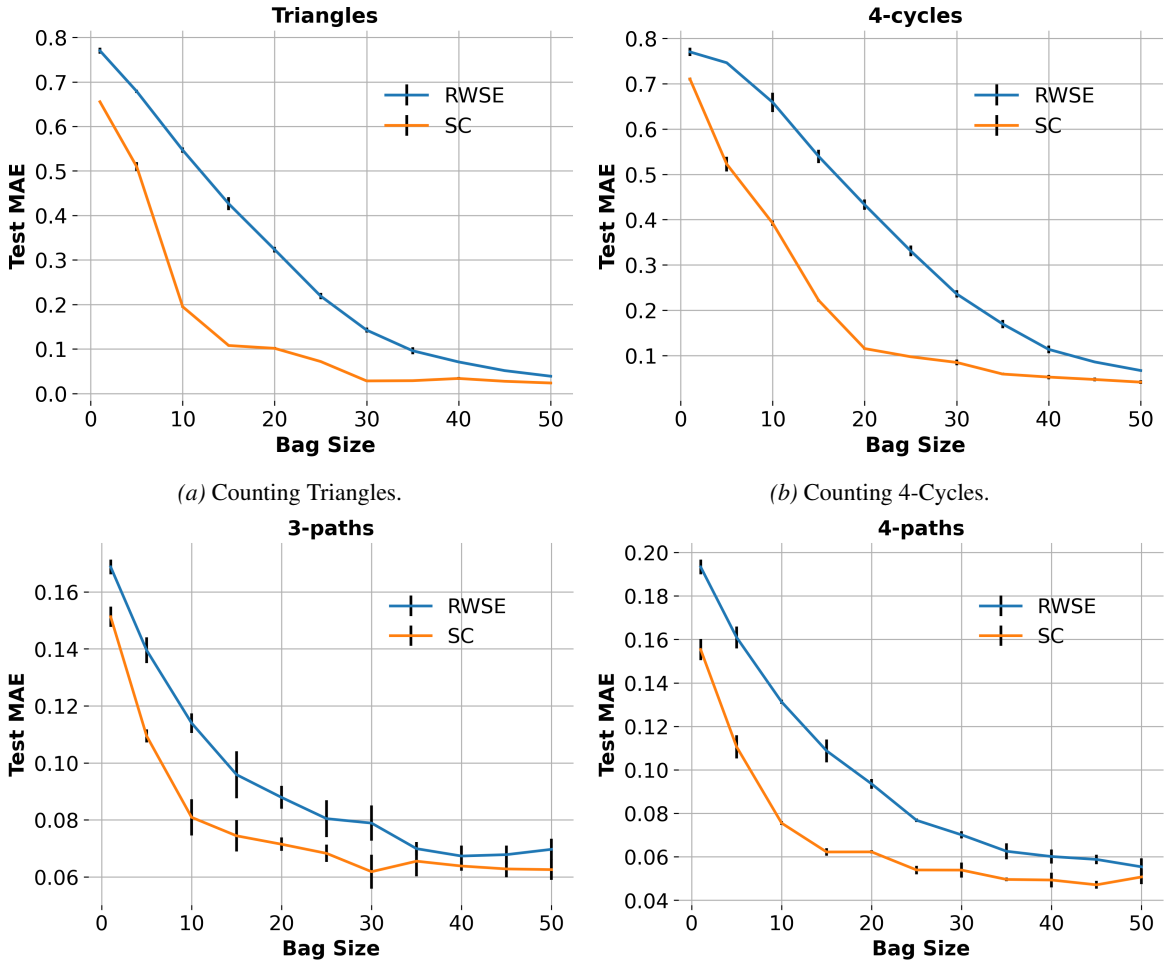

(a) Counting Triangles.

(b) Counting 4-Cycles.

(c) Counting 3-Paths.

(d) Counting 4-paths.

Figure 9: Comparing our centrality sampling with RWSE sampling for counting different substructures on synthetic random graphs.

G.1. Architectural Form

We always employ a reference Subgraph GNN architecture f whose output, for an input graph $G = (A, X, E)$[12] associated with node-marked bag B, is given by:

$$y_G^B = f(B(G)) = \phi^{(L+1)}\big(\sum_{v \in G}(h_{G,v}^{(L)} + \sum_{S \in B} h_{S,v}^{(L)})\big) \tag{45}$$

$$h_{S,v}^{(l)} = \mu^{(l)}\big(A, H_S^{(l-1)}, \eta_e(E), M_{:,S}\big)_v \tag{46}$$

$$h_{S,v}^{(0)} = [\eta_x(X)_{v,:}, C_{v,:}^{\mathsf{CSE}}] \tag{47}$$

where $\phi^{(L+1)}$ is a final prediction module and $h_{G,v}^{(L)}, h_{S,v}^{(L)}$ refer to the representations of generic node v on the original graph G and subgraph S. As it is evident from Equation (45), we employ an "augmented policy" which always includes a copy of the original graph in the bag of subgraphs (Bevilacqua et al., 2021). As we only consider node marking policies, this copy only differs from (sub)graphs in B by the fact that no nodes are marked. Representations $h_{G,v}^{(L)}, h_{S,v}^{(L)}$ are obtained à la DS-GNN (Bevilacqua et al., 2021), that is, by running independent message-passing μ on each (sub)graph independently (see Equation (46)). Note that μ explicitly processes available edge features (E) and marking information (M, see Algorithm 1). As it will be specified later on, we always consider either GIN (Xu et al., 2018) or GCN (Kipf &

[12] E is a tensor storing edge features.

Table 17: Results on ZINC and Peptides datasets showing the effect of CSEs on both GIN and HyMN.

Method	ZINC (MAE ↓)	Peptides-Func (AP ↑)	Peptides-Struct (MAE ↓)
GIN Xu et al. (2018)	0.163 ±0.004	0.6558 ±0.0068	0.2497 ±0.0012
GIN+CSE	0.092 ±0.002	0.6619 ±0.0077	0.2479 ±0.0011
HyMN (GIN, T=1) w/out CSE	0.125 ±0.004	0.6758 ±0.0050	0.2466 ±0.0010
HyMN (GIN, T=1)	0.080 ±0.003	0.6857 ±0.0055	0.2464 ±0.0013

Welling, 2017) as MPNN backbones. Equation (47) specifies initial node features for node v in subgraph S. Finally, η_x, η_e are dataset-dependent node- and edge-feature encoders, and that C^{CSE} is computed according to Algorithm 1.

Note that, across all molecular benchmarks, the GIN layer we use resembles the GINE architecture (Hu et al., 2020c), but concatenates the marking information as follows:

$$h_{S,v}^{(l)} = \phi^{(l)}\Big((1+\epsilon^{(l)})[h_{S,v}^{(l-1)}, M_{v,S}] + \sum_{u\in N(v)} \big[\sigma\big(h_{S,u}^{(l-1)} + \eta_e(E)_{vu}\big), M_{u,S}\big]\Big) \tag{48}$$

where $M_{v,S}$ is the mark for node v in subgraph S, $\eta_e(E)_{vu}$ refers to the encoded edge features for node-pair v, u, and σ is a ReLU non-linearity. As for our GCN (Kipf & Welling, 2017) backbones, the marking information is simply provided in the input of the network, and edge features are discarded.

G.2. Synthetic Experimental Details

G.2.1. Dataset Generation

For the synthetic counting substructures experiment, we generated a dataset of random unattributed graphs in a similar manner to (Chen et al., 2020). In their experiments, they generate 5000 random regular graphs denoted as $RG(m, d)$, where m is the number of nodes in each graph and d is the node degree. Random regular graphs with m nodes and degree d are sampled and then m edges are randomly deleted. In their work, Chen et al. (Chen et al., 2020), uniformly sampled (m, d) from $(10, 6), (15, 6), (20, 5), (30, 5)$. However, we want to test the effectiveness of our sampling approach for larger sizes of graphs. Additionally, we found that the number of substructures present in the graph was related to the graphs size (see Figure 10). Therefore, we wanted to create a more challenging benchmark with larger graph sizes. Therefore, we set (m, d) to be $(60, 5)$ for all graphs.

G.2.2. Synthetic Model Parameters

For our synthetic experiments, we set the base GIN to have a batch size of 128, 6 layers of message-passing, embedding dimension 32, and Adam optimizer with initial learning rate of 0.001 as prescribed by (Bevilacqua et al., 2024). We trained for 250 epoch and took the test Mean Absolute Error (MAE) at the best validation epoch.

G.3. Real-World Experimental Details

In this section, we provide further details about our experiments. We implemented our method using Pytorch (Paszke et al., 2019) and Pytorch Geometric (Fey & Lenssen, 2019). For the GIN model (Xu et al., 2018), we use Batch Normalization and the MLP is composed of two linear layers with ReLU non-linearities. Additionally, we use residual connections in each layer. The test performance at the epoch with the best validation performance is reported and is averaged over multiple runs with different random seeds. All the benchmarking results, including the extra ablations, are based on 5 executed runs, except for Peptides-func and Peptides-struct which are based on the output of four runs. In all our experiments we used AdamW (Loshchilov & Hutter, 2019), together with linear warm-up increase of the learning rate followed by its cosine decay. Experimental tracking and hyper-parameter optimisation were done via the Weights and Biases platform (wandb) (Biewald et al., 2020). In Table 2, the number of subgraphs used (T) was selected to match the choices made in other baselines, such as PL, making the comparisons as informative as possible. In Table 3 and Table 8, we chose T to be the smallest possible value, i.e., $T = 1$. This is justified by our focus on efficiency. Specific hyper-parameter information for each dataset can be found in the corresponding subsection.

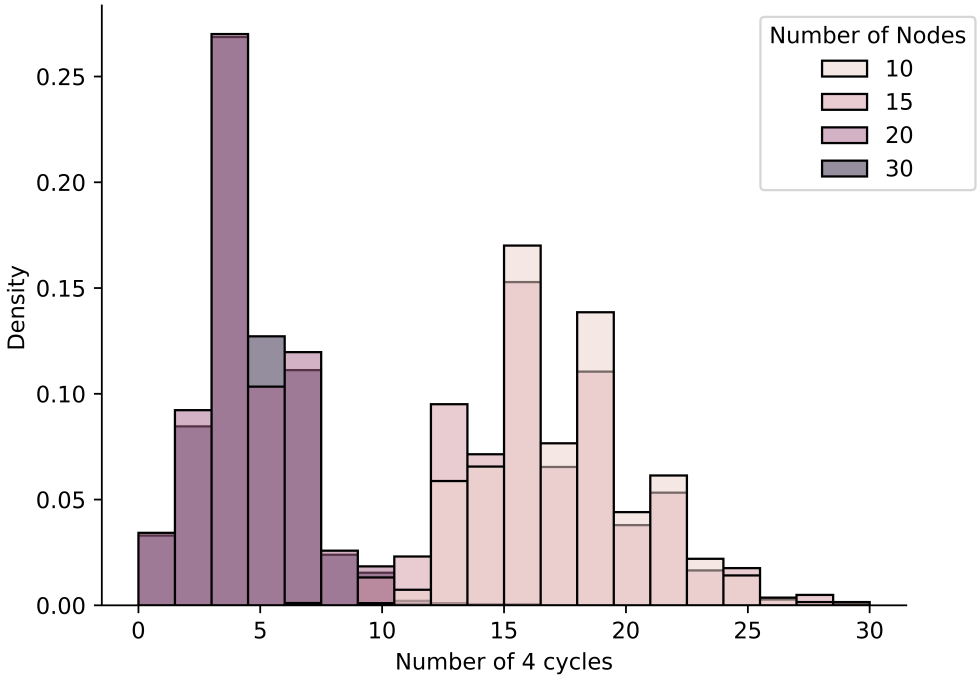

Figure 10: Evaluating the dependency between the graph size and the number of 4-cycles in the dataset generated from Chen et al. (Chen et al., 2020).

G.3.1. Hardware

All experiments were run on a single NVIDIA GeForce RTX 3080 with 10GB RAM.

G.3.2. Dataset Specific Details

Below, we provide descriptions of the datasets on which we conduct experiments.

OGB datasets (MIT License) (Hu et al., 2020b). These are molecular property prediction datasets which use a common node and edge featurization that represents chemophysical properties. MOLHIV, MOLBACE and MOLTOX21 all represent molecule classification tasks. We considered the challenging scaffold splits proposed in (Hu et al., 2020a). We set the batch size to 128 for MOLHIV and 32 for the other benchmarks to avoid out-of-memory errors. We set the hidden dimension to be 300 for all datasets as done in Hu et al. (2020a) and Bevilacqua et al. (2024). We tuned the number of layers in $2, 4, 6, 8, 10$, the number of layers post message-passing in $1, 2, 3$, dropout after each layer in $0.0, 0.3, 0.5$, whether to perform mean or sum pooling over the subgraphs, and whether to apply Batch Normalization after message-passing on each dataset. Additionally, for the method with structural encoding, we tune the number of steps k in the encoding in $16, 20$ and the dimension after the linear encoding in $16, 28$ as done in (Rampášek et al., 2022). The tuning was done on a single run for each set of hyper-parameters and the results were outlined for the best performing parameters on the validation set over 5 random seeds. These parameters are shown in Table 18.

The maximum number of epochs is set to 100 for all models and the test metric is computed at the best validation epoch.

Peptides-func and Peptides-struct (CC-BY-NC 4.0) (Dwivedi et al., 2022). These datasets are composed of atomic peptides. Peptides-func is a multi-label graph classification task where there are 10 nonexclusive peptide functional classes. Peptides-struct is a regression task involving 11 3D structural properties of the peptides. For both of these datasets, we used the tuned hyper-parameters of the GINE model from Tönshoff et al. (Tönshoff et al., 2023) which has a parameter budget under 500k and where they use 250 epochs. For both of these datasets we set the number of steps of our centrality encoding to be 20, aligned with the number of steps used for the random-walk structural encoding. The additional parameter

Table 18: Best performing hyperparameters in Table 2.

Hyperparameter	MOLHIV	MOLBACE	MOLTOX21
#Layers	2	8	10
#Layers readout	1	3	3
Hidden dim	300	300	300
Dropout	0.0	0.5	0.3
Subgraph pooling	mean	mean	sum
Positional Encoding Steps	16	20	20
PE dim	16	16	28
#Parameters	419,403	1,691,329	2,061,322

tuning which we performed was whether to do mean or sum pooling over the subgraphs. We show the best performing hyperparameters from Table 3 in Table 19.

Table 19: Best performing hyperparameters in Table 3.

Hyperparameter	Peptides-Func	Peptides-Struct
#Layers	8	10
#Layers readout	3	3
Hidden dim	160	145
Dropout	0.1	0.2
Subgraph pooling	sum	sum
Positional Encoding Steps	20	20
PE dim	18	18
#Parameters	498,904	496,107

ZINC (MIT License) (Dwivedi et al., 2023). This dataset consists of 12k molecular graphs representing commercially available chemical compounds. The task involves predicting the constrained solubility of the molecule. We considered the predefined dataset splits and used the Mean Absolute Error (MAE) both as a loss and evaluaton metric. We chose to have 10 layers of massage-passing, 3 layers in the readout function, a batch size of 32, 1000 epochs and a dropout of 0 to replicate what was done in (Rampášek et al., 2022). We altered the hidden dimension to be 148 in order to be closer to the 500k parameter budget. No further parameter tuning was done and our best performing parameters are shown in Table 20. The test metric is computed at the best validation epoch.

Table 20: Best performing hyperparameters in Table 8.

Hyperparameter	ZINC
#Layers	10
#Layers readout	3
Hidden dim	148
Dropout	0.0
Subgraph pooling	mean
Positional Encoding Steps	20
PE dim	18
#Parameters	497,353

MalNet-Tiny (CC-BY license) This dataset comprises of function call graphs derived from Android APKs. The dataset used is a subset of MalNet and contains $5,000$ graphs of up to $5,000$ nodes, coming from benign software or 4 types of malware. The task is to classify the type of software based on its structure.

REDDIT-BINARY (CC-BY license) The dataset consists of social networks posts are connected by an edge if the same user comments on both. This dataset is large in size, containing 232,965 posts with an average degree of 429. The task is to predict whether the graph belongs to a question/answer-based community or a discussion-based community. We used the evaluation procedure proposed in Xu et al. (2018), consisting of a 10-fold cross-validation and a metric with the best averaged validation accuracy across the folds.

Table 21: Best performing hyperparameters in Table 4.

Hyperparameter	MalNet-Tiny
#Layers	5
#Layers readout	3
Hidden dim	96
Dropout	0.0
Subgraph pooling	sum
Positional Encoding Steps	20
PE dim	28
#Parameters	

Table 22: Best performing hyperparameters in Table 5.

Hyperparameter	RDT-B
#Layers	2
#Layers readout	1
Hidden dim	300
Dropout	0
Subgraph pooling	mean
Positional Encoding Steps	16
PE dim	16
#Parameters	274204

H. Additional Time Comparisons

As well as Table 3 where we compared the runtime of different methods on Peptides datasets, we extend this analyses to both ZINC and MOLHIV. To this end, we provide some results in Table 23 and Table 24. We find that our method significantly improves over the baseline GIN on both of these tasks whilst having a substantially reduced runtime compared to the GPS which uses a Transformer layer. Again, this highlights both the efficiency and practical utility of our method.

Table 23: Results on the ZINC dataset with timing comparisons using a GeForce RTX 2080 8 GB.

Method	Precompute (s)	Train (s/epoch)	Test (s)	Test MAE (↓)
GIN	0.00	12.65	0.33	0.163
HyMN (GIN, T=1)	21.41	17.95	0.42	0.080
GPS (Rampášek et al. (2022))	19.13	33.02	0.87	0.070

Table 24: Results on the MOLHIV dataset with timing comparisons using a GeForce RTX 2080 8 GB.

Method	Precompute (s)	Train (s/epoch)	Test (s)	ROC-AUC (↑)
GIN	0.00	7.50	0.33	75.58
HyMN (GIN, T=1)	67.43	9.09	0.37	80.36
GPS (Rampášek et al. (2022))	40.92	124.08	4.14	78.80